# BEAMS WITH WEB OPENINGS: ULTIMATE LOAD TESTS AND DESIGN EXAMPLE

by

RICHARD LYNN KUSSMAN

B.S., Kansas State University, 1974

---

A MASTER'S THESIS

submitted in partial fulfillment of the

requirements for the degree

MASTER OF SCIENCE

Department of Civil Engineering

KANSAS STATE UNIVERSITY
Manhattan, Kansas

1975

Approved by:

Peter B. Cooper
Major Professor

# TABLE OF CONTENTS

**THIS BOOK CONTAINS SEVERAL DOCUMENTS THAT ARE OF POOR QUALITY DUE TO BEING A PHOTOCOPY OF A PHOTO.**

**THIS IS AS RECEIVED FROM CUSTOMER.**

TABLE OF CONTENTS (Continued)

LIST OF TABLES

LIST OF FIGURES

LIST OF FIGURES (Continued)

# INTRODUCTION

Due to the increasing cost of energy and the difficulty of obtaining raw materials, economy has a high priority in all aspects of design. In the design of multistory steel buildings, savings can be realized by passing ductwork for heating, ventilation, and air conditioning systems through steel floor beams rather than under them. Not only does this practice save in the overall height of the structure along with related benefits in material savings, but it also saves in the cost of heating and air conditioning by enclosing less volume to be heated or cooled. Eccentric openings are of special interest because not all floor beams and girders are of the same depth at any given level. It is desirable to keep the ductwork on a relatively level plane to cut down on the cost of fabricating vertical bends. It is doubtful that it costs any more to fabricate an eccentric opening in a steel beam than it does to fabricate a concentric opening. Thus, even more savings can be realized by using the eccentric opening. The addition of reinforcement is also sometimes desirable so that with the opening, a heavier section is not required.

Past experimental programs that included ultimate load tests have been carried out by Bower [1] and Redwood and McCutcheon [2] for unreinforced, concentric openings, by Cooper and Snell [3] and Congdon and Redwood [4] for reinforced, concentric openings, and by Frost [5] for unreinforced, eccentric openings. In Part I of this thesis tests on W-shape steel beams with reinforced, eccentric openings in the webs are described and discussed. The moment-to-shear ratio and the eccentricity were held constant at 30 and 2 inches, respectively in the tests, while the reinforcement, opening length, and opening depth were the primary test variables. The main objectives of this experimental investigation were to observe the behavior of steel beams with reinforced, eccentric

web openings under ultimate load conditions, and to obtain ultimate load data to compare with the results of a previously developed theoretical analysis.

Design procedures have been developed for beams with concentric web openings, both unreinforced and reinforced [6,7,8], however none were available for beams with eccentric web openings. Until recently, no design formulas were available for reinforced, eccentric web openings, so no design procedures had been developed. In Part II of this thesis an example is presented to illustrate the use of these formulas in the design of part of a building floor system.

# PART I: ULTIMATE LOAD TESTS

## TEST SPECIMENS

Five ultimate load tests were conducted; two on W 16 x 45, A36 steel beams and three on W 16 x 40, A36 steel beams. Although the length of the beams varied somewhat, the moment-to-shear ratio at the centerline of the opening, M/V, was held constant at 30 inches. The test setup, as depicted in Fig. 1a, consisted of simple supports at the ends and a concentracted load applied at midspan. A variable, X, describes the variation of the span length as illustrated in Fig. 1a and tabulated in Table 1 for the various test specimens. Beams 3 and 4 are not listed in Table 1 since they were subjected to elastic tests only.

The size of the openings in the beams was one of the experimental variables. As shown in Fig. 1b, the opening size is defined by half the opening length, a, half the opening depth, h, and the corner radius, r. The values of these variables for each of the test specimens can be found in Table 1. For this test program, the opening eccentricity, which is the distance between the mid-depth of the beam and the centerline of the opening, was kept constant at 2 inches. The eccentricity was toward the compression flange in beams 1, 2, and 5 and in beams 6 and 7, it was toward the tension flange.

For the first two beams, the openings were fabricated by a commercial fabricator, who flame-cut them with the aid of a machine template. The openings in the other three beams were fabricated in the Civil Engineering Shop at Kansas State University by drilling holes at each of the four corners and then flame-cutting the sides of the opening along a line tangent to the drilled holes with a hand-held torch guided along a straight edge.

The openings in all the beams except Beam 1 had some type of reinforcement. In Fig. 1b, the general layout of the reinforcement used in each case is shown. The reinforcement consisted of bars above and below the opening on either one or both sides of the web as described in Table 1. Because of the width-thickness ratio limitations of the AISC Specification [9], a Bar 2 x 1/2 was considered the practical minimum size for the reinforcing bars. In all cases the reinforcing bars extended 3" beyond the edges of the openings. Three inch extensions were selected because this was the length required to develop the strength of the bar using a 3/16 inch fillet weld. In all the beams the reinforcing bars are welded continuously along the opening side of the bar and returned 1 1/2 inches on the flange side of the bar at both ends with a 3/16 inch fillet weld. As shown in Fig. 1b, the distance from the edge of the opening to the edge of the reinforcing bars was always 1/4 inch.

During an initial test on Beam 1, a slight amount of web crippling was detected at midspan under the load point, so the test was stopped, and bearing stiffeners were added at midspan. In all other cases bearing stiffeners were provided at the supports and at the load points to avoid further web crippling problems. These bearing stiffeners were all Bar 3 x 1/4's, and were welded with 3/16 inch fillet welds to the web. Full bearing was provided between the stiffener ends and the flanges to which loads or reactions were applied.

In Beams 2 and 5 cover plates were used on the top and bottom flanges in the center portion of the beam to increase the plastic section modulus and thereby force the failure to occur at the opening rather than at midspan. Table 1 lists the sizes of cover plates used for these beams. Because the opening sizes, reinforcement, and spans used were such that failure could occur at the opening before a plastic hinge could form at midspan in Beams

1, 6, and 7, cover plates were not required. In the beams where cover plates were needed, they were welded to the top and bottom flanges with 1/4 inch fillet welds all around their edges.

Before the beams were tested, the cross section dimensions were measured at each end. These measurements were averaged and the results can be found in Table 2 where they are compared with the nominal dimensions.

Standard tensile test specimens were cut from the beam and reinforcing bars to determine the actual static yield points. Two coupons were taken from the web, the reinforcing bar stock, and from each flange. In Table 3, the average yield point and maximum deviation from the average are listed for each beam.

Cross-sectional properties relative to the ultimate strength analysis, based on the average dimensions, are also presented in Table 3. These properties are $A_v$, the shear area (web thickness times total depth), and Z, the plastic section modulus. The contributions of the flange-web fillets to the plastic section modulus was included by adding the difference between the computed plastic section modulus using nominal dimensions and the handbook value (see Appendix III). Also listed in Table 3 are the plastic shear force, $V_p$, defined as the shear yield stress ($F_y/\sqrt{3}$) times $A_v$, and the plastic moment, $M_p$ (yield stress times plastic section modulus).

## TEST SETUP AND INSTRUMENTATION

For the tests, a Tinius-Olsen screw type machine with a 200 kip capacity was used. The load was measured by a lever type load balancing arm and pedestal supports were placed on the cantilever arms of the machine to serve as end supports for the beams.

The supports were rounded at the point of contact with the beam to give essentially a knife-edge support. Additionally, the inside edges of the support bases were slightly rounded, thus permitting the supports to rock inward as the test beams were deformed under load. Bearing plates were used between the beam and the support and also between the beam and the bearing block of the machine. At the supports, PL's 1 x 3 x 7 were used while a PL 1 x 6 x 7 was used at the load point.

The loads were applied at midspan through a spherical bearing block attached to the moveable crosshead of the testing machine. As noted above, a bearing plate was used between the bearing block and the beam. Lateral support was supplied to the compression flange at the load point by friction between the beam and the bearing block. At the end supports, lateral support was applied to the tension flange through friction between the beam and the pedestal supports. For beams 2, 5, 6, and 7, this support was transmitted to the compression flange by the bearing stiffeners provided at the supports.

Deflections were measured by mechanical dial gauges with division of one-thousandth of an inch (0.001 inch) and a maximum stroke of 2 inches. Support of the dial gauges was provided by a 4 inch channel, 18 feet in length resting on the pedestal supports. This arrangement made it unnecessary to correct the dial gauge readings for settlement of the

supports. Deflection data was obtained for the beam at midspan under the load and at both edges of the opening.

A coat of whitewash was applied to all surfaces of the beams prior to testing. When yielding occurs, the whitewash cracks and flakes off along with the mill scale leaving a visible record. During the tests it was evident that whitewash flaking was much more pronounced in regions subjected to compressive stresses than those in tension. This behavior has also been observed by other investigators [2]. The cracking and flaking, however, provides only a qualitative estimate of the yielding. By providing greater contrast with the background the whitewash was also an aid in taking photographs of the test beams.

## TEST PROCEDURE

During the initial portion of the tests load increments were selected in an attempt to obtain at least three points on the load-deflection curves in the elastic range. When a load was reached in this portion of the test, the three deflection readings were recorded along with the load. Loading was then resumed. The changes in deflections in the load versus both relative opening and midspan deflection curves for increment between Loads 1 and 2 were, in general, not linear relative to subsequent intervals in the elastic range. This can be seen by observing Figs. 2 through 11. The non-linearity in the first interval is due to the beam seating itself on the supports. A study of the load-deflection curves for the test beams will reveal a greater deviation from linearity in this zone for Beams 6 and 7. This greater departure is born out by visual observations prior to the tests that in both cases one end of the beam was twisted slightly relative to the other end.

During the test on Beam 5, it was observed at Load 8 that the limit switches, which control crosshead movement on the testing machine, would have to be adjusted before the test could be completed. As indicated in Figs. 4 and 9, the load was completely removed, at Load 9, to permit the limit switches to be adjusted, after which the test was resumed.

In the strain hardening zone of the inelastic range it was attempted to obtain at least three points in a straight line prior to reaching the ultimate load. In this portion of the load-deflection curves, constant deflection increments were used between points where readings were taken. Once a specified deflection was reached the three dial gauge readings were recorded along with the load. The load was then allowed to drop-off for eight to ten

minutes. This drop-off time is approximately the same time lapse between the dynamic and static loads used in the tensile coupon tests to determine the static yield point. While the load was dropping off, zones of yielding were noted as indicated by the flaking whitewash. Once the load had dropped off for the specified length of time, the new load was recorded and loading was resumed. The deflections remained relatively constant when loading was stopped because of the screw-type machine being used. The test was terminated when there was an obvious reduction in load-carrying capacity.

Dynamic load is the term used to describe the load the beam is carrying while the testing machine crosshead is moving. This load is indicated in Fig. 2 as the top of the vertical line at each load point. After the load had dropped off for eight to ten minutes, the static load was noted. On the bottom tip of the vertical line used to describe the dynamic load, the static load is circled. This same scheme is used in all the load-deflection curves.

# PRESENTATION AND DISCUSSION OF RESULTS

## Ultimate Loads

Two experimental values of the ultimate load were obtained for each beam. The first was the largest static load reached during the test. The second is the experimental ultimate load corrected for strain hardening. These experimental results are presented in Table 4, along with a theoretical prediction of the ultimate load. Since the effects of strain hardening are not considered in the theory, it is appropriate to compare the corrected experimental ultimate load with the theoretical. The ratios of these values, also listed in Table 4, indicate that the theory provides a reasonably good prediction of the load-carrying capacity of the test beams.

The corrected experimental ultimate loads were found by extending the linear portions of both the elastic region and the strain hardening region. The ordinate of the point where these two extensions intersect is the experimental ultimate load corrected for strain hardening. Although somewhat approximate, this method does provide a means of eliminating the effects of strain hardening and has also been utilized by another investigator [5]. Two types of plots were used for each beam to establish the correction. One was the load-versus-midspan deflection curves as in Figs. 2 through 6. The other was the load-versus-relative opening deflection curves shown in Figs. 7 through 11. Usually the latter was merely an independent check, but in the case of Beam 7, it was needed to make a decision as to which segment of the strain hardening range should be used.

The theoretical ultimate load can be found through the use of an interaction diagram similar to the one in Fig. 13. A ratio of the shear force

(V) to the plastic shear force ($V_p$) is assumed. Using this $V/V_p$ ratio and the moment to shear force ratio (M/V), the moment-to-plastic moment ($M/M_p$) ratio is calculated. Now the coordinates of one point on a ray representing the given M/V ratio are known. This ray is formed by passing a straight line from the origin through the point. Where the ray intersects the interaction curve are the coordinates of $V/V_p$ and $M/M_p$ corresponding to failure at the opening. The moment (M) is determined from the $M/M_p$ coordinates and using the M/V ratio, the theoretical ultimate load is calculated. An example of these calculations can be found in Appendix III.

The interaction diagram used to predict the theoretical load was plotted using coordinates compiled from Wang's computer program for beams with eccentric, reinforced web openings [10]. In Figs. 12 through 14, the interaction diagrams show the points representing the experimental ultimate loads. The $M/M_p$ and $V/V_p$ coordinates for these ultimate loads can be found in Table 4. In all but one case, the ultimate load corrected for strain hardening fell outside the failure envelope, and in all cases the corrected ultimate loads were quite close to the failure envelopes.

## Yield Patterns and Modes of Failure

Before getting into the specific yield patterns and modes of failure for each of the beams, a few general comments are in order. First, extensive elastic tests were conducted on Beams 1, 2, and 5 before the ultimate load tests [11,12]. In the elastic tests a large number of strain gauges were used on the sections above and below the openings near the opening edges. Prior to attaching the strain gauges, the mill scale had to be ground off. Therefore, the whitewash used as an indicator of yielding in the ultimate

load tests did not flake off as easily in these beams as in Beams 6 and 7. In all the tests, the first signs of yielding were observed in the web adjacent to the corners or edges of the openings. These yielded zones were typically enlarged as the tests progressed. Failure of all the test beams can be attributed to some type of instability of the compression flange after the ultimate load was exceeded.

Two ultimate load tests were conducted on Beam 1. The first was halted prematurely because of slight web crippling under the load point at midspan. No yielding was evident until the web crippling began, and then some minor yielding was noted at the top corner of the low moment edge of the opening. At this point the test was barely in the inelastic range. Testing was stopped and the beam unloaded. The beam was then repositioned on the supports to maintain the same moment-to-shear ratio (M/V) but with the crippled web just inside one end support. This repositioning was possible because of the length of beam required for the various M/V ratios used in the elastic tests [11]. Bearing stiffeners were welded to the beam at the new load point to prevent web crippling in the second test. This solution was also adopted for all subsequent test beams, and no further web crippling problems were encountered.

During the second ultimate load test on Beam 1, the first yielding was observed at the corners of the high moment edge of the opening at a load level less than the corrected ultimate load. As the test continued, the yielding increased at the high moment edge and spread toward midspan. Yielding was also extensive between the opening and the tension flange, with a minor amount at the low moment corners. The final pattern can be seen in Fig. 15a.

Failure of Beam 1 was by lateral torsional buckling of the compression flange. The displacement of the compression flange relative to the tension flange adjacent to one support was in excess of 2 inches at Load 11 as shown in Fig. 15b. Once the load was removed, most of this displacement was recovered. In all subsequent test beams, bearing stiffeners were provided at the supports, which in turn provided lateral support to the compression flange at these points. In comparing the load-versus-relative opening deflection curve with the midspan load-deflection curve for Beam 1 with those for Beam 2, Figs. 2, 3, 7, and 8, it can be concluded that Beam 1 never actually failed at the opening because of the lateral buckling failure. Furthermore, the calculated ultimate load for failure by formation of a plastic hinge at midspan was very close to the theoretical ultimate load for failure at the opening. Therefore, there is some uncertainty as to whether the ultimate load corresponding to opening failure was actually attained.

Beam 2 was supplied with cover plates at midspan to increase the plastic section modulus and thereby force the failure to occur at the opening. Bearing stiffeners were also provided at the load point and the two support points for Beam 2 and for all subsequent tests. Initial yielding was observed at the bottom corner of the high moment edge of the opening. As the load was increased zones of yielding extending away from the opening began to develop in the web between the reinforcing bars on both sides of the opening. This general yield pattern can be seen in Fig. 16a.

When the test had progressed to within one load increment of the ultimate load, some lateral deflection of the compression flange near the high moment edge of the opening was noted. As the loading was increased, this buckling became more severe. At the end of the test a slight web buckle had also developed at the high moment end of the opening between the reinforcing bars

as shown in Fig. 16b. The final mode of failure appeared to be a combination of lateral and local buckling of the compression flange. A careful study of Fig. 16a, taken after completion of the test, will reveal the shear deformation of the opening. This type of deformation is associated with the four-hinge failure mechanism assumed in the theoretical analysis [10], and can be seen graphically in Fig. 8.

Beam 5 was the only beam in the test program to have reinforcement on both sides of the web, which significantly increased the strength of the opening. Because of the increased load carrying capacity at the opening, cover plates were required at midspan to insure a failure at the opening. The first yielding noted during the test was in the web between the reinforcing bars on both sides of the opening at Load 6. As the test progressed, the zones of initial yielding grew and spread away from the opening. The next new point of yielding was found over the high moment edge of the opening in the compression flange. Near the end of the test, at Load 13, a noticeable dip in the compression flange began to develop at this same section. The final new area of yielding was first noticed at Load 8 between the tension flange and the opening. Fig. 13 shows the final yield pattern of Beam 5 after unloading. Failure was attributed to local buckling of the compression flange over the high moment edge of the opening.

Beams 6 and 7 were similar in most respects. Both had openings that were eccentric toward the tension flange. The openings in both cases were 8 inches deep and reinforcement was placed on one side of the web. The only difference between the two beams was in the lengths of the openings. Because of these similarities, the yield patterns were also very similar. These yield patterns can be seen in final form in Figs. 18a and 19a.

First yielding was noted on Beam 6 in the web near the top corner of the low moment edge of the opening. This zone of yielding increased in size and spread toward the center of the opening. The web near the top corner of the high moment edge was the next area to yield. As the loading was increased, yielding developed in the compression flange above the high moment edge in the web above the opening, and finally between the reinforcing bars at the high moment edge. After first appearing, the yielding in these areas became more extensive with increasing load.

At Load 12 the first signs of local buckling in the compression flange were noticed. At this same level, a considerable amount of web buckling at the top of the low moment edge was noted. As the load was increased beyond this point the local buckling of the compression flange and the web buckling both became more severe and the former was assumed to be the final mode of failure for Beam 6. Figure 18b shows the extent of the web buckle after unloading.

In Beam 7 the yield pattern was almost identical to that for Beam 6. While yielding was not always of the same intensity as in Beam 6, the sequence and the direction of propagation were essentially identical. The final yield pattern can be seen in Fig. 19a. Failure in Beam 7 was by local buckling of the compression flange, as in Beam 6. A slight amount of lateral buckling was also present. Again, similar to Beam 6, Beam 7 had an extensive web buckle at the top of the low moment edge. This is shown in Fig. 19b.

A brief look at Figs. 18a and 19a will reveal a definite shear deformation in both Beams 6 and 7. This extensive deformation indicates that the beam failed at the opening. Furthermore, it shows that the openings formed

the four-hinge mechanisms assumed in the theoretical analysis. A study of Figs. 5 and 10 will illustrate an interesting development in Beam 6. At Load 12, the ultimate load, the relative opening deflection exceeded the midspan deflection. Also, after unloading, the low moment edge had deflected upward relative to its position when the test began. This tends to confirm that a substantial redistribution of internal forces occurred as the four-hinge mechanism was developed.

## SUMMARY

The experimental results obtained are in reasonable agreement with the theoretical results. In only one case, Beam 5, was the ultimate load corrected for strain hardening less than the theoretical ultimate load. In the other four tests, the corrected ultimate load exceeded the prediction by a maximum of 5%. The deformations and areas of yielding around the opening were consistent with the four-hinge failure mechanism assumed in the theory.

In all five beams, the load-carrying capacity was limited by some type of instability in the compression flange. Beam 1 failed by lateral torsional buckling of the compression flange. At the load level where this failure occurred, there was no evidence that a four-hinge mechanism had developed at the opening. Therefore, the measured ultimate load is somewhat lower than that associated with an opening failure. In Beams 2, 5, 6, and 7, the four-hinge mechanism did develop. This was followed by local buckling of the compression flange over the high moment edge of the opening and subsequent loss of load-carrying capacity. In Beams 1, 2, and 5, the opening was eccentric toward the compression flange. Conversely, the opening was eccentric toward the tension flange in Beams 6 and 7. The direction of eccentricity had little effect on the results as evidenced by Figs. 12 through 14. This is consistant with the theory since the ultimate load prediction is independent of the direction of eccentricity.

The length has an effect on the strength of the opening. Beams 6 and 7 both had openings 8 inches deep. The lengths were different, however, - 16 inches for Beam 6 and 12 inches for Beam 7. The experimental ultimate load for Beam 6 was 94.4 kips compared to 114.0 kips for Beam 7. This gives an increase of over 20% in strength for a 25% reduction in length. The change

in strength is not, however, linearly related to opening length. After the correction for strain hardening, the ultimate loads for Beams 6 and 7 were 84 kips and 101 kips, respectively. Even when the strain hardening is neglected, Beam 7 has an increase of over 20% in strength relative to Beam 6. Therefore, it can be concluded that the length is an important parameter in determining the strength of the opening.

For two of the test parameters, reinforcement and opening depth, no direct evidence was obtained from the tests showing their contribution to the strength of the opening. In Beam 2 the effects of the reinforcing bars on the opening strength could not be evaluated because of the premature failure of Beam 1 with an unreinforced opening of the same size. Beams 5 and 7 had the same opening length with different depths - 6 and 8 inches, respectively. Beam 5, however, also had more reinforcement than Beam 7. Therefore there is not enough experimental data to assign relative contributions to the respective variables. The manner in which reinforcement and opening depth affect the strength of the opening can, however, be shown indirectly. The experimental results for eccentric, unreinforced openings reported by Frost [5] and those for eccentric, reinforced openings contained in this report show reasonably good agreement with the theoretical analyses. Since the theory shows an increase in opening strength for both additional reinforcement and shallower opening depth and the theory has been shown to compare favorably with experimental results, then the addition of reinforcement and the reduction in opening depth must in practice increase the opening strength.

# PART II: DESIGN EXAMPLE

## PROBLEM STATEMENT

A portion of the floor system supporting a concourse in a multi-story building is shown in Fig. 20. The floor system consists of girders spanning from column to column with floor beams supported by the girders. The floor beams and girders support a 4-inch concrete slab which in turn provides continuous lateral support to the top flanges of the floor members. Moment connections are provided between the columns and girders, and therefore the girder ends are assumed to be fixed. It is further assumed that the columns are W14 sections and the girder span is taken from column face to column face. The floor beams are attached to the girders with shear connections and simple supports are therefore assumed. For architectural reasons the floor beams are limited to a 21-inch depth.

The heating, ventilation, and air conditioning (HVAC) ducts run parallel to the girders with service ducts branching out at right angles. For both architectural and aesthetic reasons it is undesirable to run the HVAC system below the floor members, so they must penetrate them. It is also desirable to keep the HVAC system on a level plane, thereby reducing installation costs by decreasing the number of bends in the duct material. It is necessary to provide a duct area of 144 square inches with 1-inch thick insulation on all sides. Vertical positioning of the ducts used in this example are shown in Fig. 21. The corner radius was determined from recommendations for members subjected to fatigue loadings [6]. While structures designed by plastic methods are not subject to fatigue situations, these guidelines were used to provide a reasonable basis for determining the corner radii of web openings. It is also possible that a slightly smaller opening could have been used to accommodate the duct. The use of a smaller opening might,

however, cause problems in the installation of the duct insulation and thereby increase costs. A liberal clearance was therefore provided in this example.

The floor system is to be designed to carry a live load of 100 psf [13] and a dead load of 80 psf (50 psf for the concrete slab and 30 psf for other dead loads). Using A36 steel and the AISC Specification for plastic design along with current research results, the locations where openings can be placed along the length of the floor beams and girders will be explored with the opening reinforcement varying as follows: (1) no opening reinforcement is provided; (2) enough reinforcement is supplied to resist the maximum shear force in the beam; and (3) the minimum reinforcement required to develop the shear strength of the section is furnished.

## FLOOR BEAMS

### Selection of Beam Section

Uniformly Distributed Load: $w = (1.7)(12)(0.10 + 0.08) = 3.67$ kips/ft.

Design Moment: $M = (3.67)(35)^2/8 = 562$ kip-ft.

Required Plastic Section Modulus: $Z = (562)(12)/36 = 187$ in$^3$

Try W21 x 82 ($Z = 192$ in$^3$ > 187 in$^3$)

Design Shear: $V = (3.67)(35)/2 = 64.2$ kips

Plastic Shear Force: $V_p = (0.55)(36)(20.86)(0.499) = 206$ kips > 64.2 kips

| Use W21 x 82 |
|---|

### Properties for Investigating Local Strength at the Opening

Opening Parameters: $h = 6$ in. $\quad a = 9.5$ in. $\quad e = 0$

Cross Section Properties: $A_f = (8.962)(0.795) = 7.12$ in$^2$

$A_w = (20.86)(0.499) = 10.4$ in$^2$

Reference Values: $M_p = (192)(36)/12 = 576$ kip-ft.

$V_p = 206$ kips (from above)

### Calculation of Internal Beam Forces

The internal beam forces are described by the two expressions below which were obtained from Fig. 22. These forces are plotted in Fig. 23 along with the interaction diagrams for the floor beams.

$$\left|\frac{V}{V_p}\right|_x = \frac{64.2 - 3.67x}{206}$$

$$\left|\frac{M}{M_p}\right|_x = \frac{64.2x - 1.84x^2}{576}$$

## Opening Locations for $A_r = 0$

Calculation of interaction diagram coordinates using formulas presented in Appendix IV with $A_r = e = 0$:

$$\alpha = \left(\frac{3}{16}\right)\left(\frac{20.86}{9.5}\right)^2\left(1 - \frac{12}{20.86}\right)^2 = 0.163$$

$$\beta = \frac{10.4}{(2)(7.12)}\left[\left(1 - \frac{12}{20.86}\right)^2 \frac{1}{1.163}\right]^{1/2} = 0.288$$

$$\left(\frac{M}{M_p}\right)_0 = \frac{1 + \frac{10.4}{7.12}\left[\frac{1}{4} - \left(\frac{1}{20.86}\right)^2\right]}{1 + \frac{10.4}{(4)(7.12)}} = 0.911$$

$$\left(\frac{M}{M_p}\right)_1 = \frac{1 - 0.288}{1 + \frac{10.4}{(4)(7.12)}} = 0.522$$

$$\left(\frac{V}{V_p}\right)_1 = 2\left[\left(\frac{1}{2} - \frac{6}{20.86}\right)^2 - \left(\frac{7.12}{10.4}\right)^2 (0.288)^2\right]^{1/2} = 0.158$$

The above coordinates are plotted to form the approximate interaction diagram shown in Fig. 23 for $A_r = 0$. As shown schematically in Fig. 24a and graphically in Fig. 23, there are no positions along the beam where the opening can be placed for $A_r = 0$. This is because all the points on the internal beam force curve lie outside the failure envelope for $A_r = 0$.

## Opening Locations for $A_r$ Large Enough to Accommodate Maximum Beam Shear

The following quadratic equation in $A_r$ is obtained from the generalized equation for $(V/V_p)_1$ presented in Appendix IV with $A_r \leq (A_r)_{min}$:

$$AA_r^2 + BA_r + C = 0$$

where

$$A = \frac{16\alpha}{A_w^2 (1+\alpha)}$$

$$B = \frac{8\alpha}{(1+\alpha)A_w}\left[\left(1 - \frac{2h}{d}\right)^2 - \left(\frac{V}{V_p}\right)^2\right]^{1/2}$$

$$C = \left(1 - \frac{2h}{d}\right)^2 \left(\frac{\alpha}{1+\alpha}\right) - \left(\frac{V}{V_p}\right)^2$$

Calculation of $A_r$:

$$V_{max}/V_p = 0.312$$

$$A = \frac{(16)(0.163)}{(10.4)^2(1.163)} = 0.0207$$

$$B = \frac{(8)(0.163)}{(1.163)(10.4)}\left[\left(1 - \frac{12}{20.86}\right)^2 - (0.312)^2\right]^{1/2} = 0.0311$$

$$C = \left(1 - \frac{12}{20.86}\right)^2 \frac{(0.163)}{(1.163)} - (0.312)^2 = -0.0721$$

$$A_r = \frac{-B \pm \sqrt{B^2 - 4AC}}{2A}$$

$$A_r = \frac{-0.0311 \pm \sqrt{(0.0311)^2 - (4)(0.0207)(-0.0721)}}{(2)(0.0207)}$$

$$A_r = 1.26 \text{ in}^2$$

| |
|---|
| Use 1-Bar 3 x 7/16 above and below the opening on one side only. |

($A_r = 1.31 \text{ in}^2 > 1.26 \text{ in}^2$ ; $b_r/t_r = 6.9 < 8.5$)

Calculation of interaction diagram coordinates using formulas presented in Appendix IV with $A_r = 1.26 \text{ in}^2$, e = 0:

$$\beta = -\frac{(2)(0.163)}{1.163}\left(\frac{1.26}{7.12}\right) + \frac{10.4}{(2)(7.12)}\left[\left(1 - \frac{12}{20.96}\right)^2 \frac{1}{1.163} - \frac{(16)(0.163)}{(1.163)^2}\left(\frac{1.26}{10.4}\right)^2\right]^{1/2} = 0.210$$

$$\left(\frac{M}{M_p}\right)_0 = \frac{1 + \frac{1.26}{7.12}\left(\frac{12}{20.86}\right) + \frac{10.4}{7.12}\left[\frac{1}{4} - \left(\frac{6}{20.86}\right)^2\right]}{1 + \frac{10.4}{(4)(7.12)}} = 0.986$$

$$\left(\frac{M}{M_p}\right)_1 = \frac{1 - \frac{1.26}{7.12} - 0.210}{1 + \frac{10.4}{(4)(7.12)}} = 0.449$$

$$\left(\frac{V}{V_p}\right)_1 = 2\left[\left(\frac{1}{2} - \frac{6}{20.86}\right)^2 - \left(\frac{7.12}{10.4}\right)^2 (0.210)^2\right]^{1/2} = 0.313$$

These coordinates are plotted in Fig. 23 to describe the center interaction diagram. It should be noted that the maximum shear in the beam is just within the failure envelope of the diagram as shown by the point on the internal beam force curve corresponding to $M/M_p$ equals zero. In the regions of higher moment part of the internal beam force curve falls outside the envelope indicating that the opening should not be placed in the areas shown in Fig. 24b with $A_r = 1.26$ in$^2$.

Opening Locations for $(A_r)_{min}$

$$(A_r)_{min} = \frac{(9.5)(0.499)}{\sqrt{3}} = 2.74 \text{ in}^2$$

> Use 1-Bar 3-3/4 x 3/4 above and below the opening on one side only.

($A_r = 2.81$ in$^2$ > 2.74 in$^2$ ; $b_r/t_r = 5.0 < 8.5$)

Calculation of interaction diagram coordinates using formulas presented in Appendix IV with e = 0, $A_r = 2.81$ in$^2$:

$$\left(\frac{M}{M_p}\right)_0 = \frac{1 + \frac{(2.81)}{(7.12)}\left(\frac{12}{20.86}\right) + \frac{(10.4)}{(7.12)}\left[\frac{1}{4} - \left(\frac{6}{20.86}\right)^2\right]}{1 + \frac{10.4}{(4)(7.12)}} = 1.08$$

$$\left(\frac{M}{M_p}\right)_1 = \frac{1 - \frac{2.74}{7.12}}{1 + \frac{10.4}{(4)(7.12)}} = 0.451$$

Note that in the above calculations for $(M/M_p)_1$, the calculated value of $(A_r)_{min}$ was used in place of the area of the bar chosen. This is because $A_r$ is subtracted from one in this equation and logic tells us that more reinforcement must increase the load carrying capacity of a member, not decrease it. Therefore the $(A_r)_{min}$ value calculated as above should be used to prevent overly conservative results.

$$\left(\frac{V}{V_p}\right)_1 = (1 - \frac{12}{20.86}) = 0.425$$

These coordinates are plotted on Fig. 23 to form the outside interaction diagram. With the reinforcing area set at $(A_r)_{min}$, the opening can be placed anywhere along the beam as shown in Fig. 24c.

# GIRDERS

## Selection of Girder Section

Load: $P = (3.67)(35) = 128$ kips

Design Moment: $M = (128)(11.4)/2 = 730$ kip-ft.

Required Plastic Section Modulus: $Z = (730)(12)/36 = 243\ in^3$

Try W27 x 84 ($Z = 244\ in^3 > 243\ in^3$)

Design Shear: $V = 128$ kips

Plastic Shear Force: $V_p = (0.55)(36)(0.463)(26.69) = 245$ kips $> 128$ kips

Use W27 x 84

## Properties for Investigating Local Strength at the Opening

Opening Parameters: $h = 6$ in. $\quad a = 9.5$ in. $\quad e = 3$ in.

Cross Section Properties: $A_f = (9.963)(0.636) = 6.34\ in^2$

$A_w = (0.463)(26.69) = 12.4\ in^2$

Reference Values: $M_p = (244)(36)/12 = 732$ kip-ft

$V_p = 245$ kips (from above)

## Calculation of Internal Beam Forces

The internal beam forces form a discontinuous curve described by the expressions below taken from Fig. 25 with the appropriate limits. This curve is shown in Fig. 26.

$$\left|\frac{V}{V_p}\right| = \frac{128}{245} = 0.522$$

$$\left|\frac{M}{M_p}\right|_x = \frac{-730 + 128x}{732}$$

Limits: $0 \leq X \leq 11.4$ ft.

where x is positive from the column face toward midspan.

$$\left|\frac{V}{V_p}\right| = 0$$

$$\left|\frac{M}{M_p}\right| = 0.997$$

} Limits: 11.4 ft. $\leq X \leq$ 17.4 ft. where x is as described above.

Opening Locations for $A_r = 0$

Calculation of interaction diagram coordinates using formulas presented in Appendix IV with $A_r = 0$, e = 3 in.:

$$\alpha_T = \frac{3}{16}\left(\frac{26.69}{9.5}\right)^2 \left(1 - \frac{12}{26.69} - \frac{6}{26.69}\right)^2 = 0.157$$

$$\alpha_B = \frac{3}{16}\left(\frac{26.69}{9.5}\right)^2 \left(1 - \frac{12}{26.69} + \frac{6}{26.69}\right)^2 = 0.889$$

$$\beta_T = \frac{12.4}{(2)(6.34)}\left[\left(1 - \frac{12+6}{26.69}\right)^2 \frac{1}{1.157}\right]^{1/2} = 0.296$$

$$\beta_B = \frac{12.4}{(2)(6.34)}\left[\left(1 - \frac{12-6}{26.69}\right)^2 \frac{1}{1.889}\right]^{1/2} = 0.552$$

$$\left(\frac{M}{M_p}\right)_0 = \frac{1 + \frac{12.4}{6.34}\left[\frac{1}{4} - \frac{(6)^2 + (2)(6)(3)}{(26.69)^2}\right]}{1 + \frac{12.4}{(4)(6.34)}} = 0.867$$

$$\left(\frac{M}{M_p}\right)_1 = \frac{1 - 0.552}{1 + \frac{12.4}{(4)(6.34)}} = 0.301$$

$$\left(\frac{V_T}{V_p}\right)_1 = \left[\left(\frac{1}{2} - \frac{6+3}{26.69}\right)^2 - \left(\frac{6.34}{12.4}\right)^2 (0.296)^2\right]^{1/2} = 0.060$$

$$\left(\frac{V_B}{V_p}\right)_1 = \left[\left(\frac{1}{2} - \frac{6-3}{26.69}\right)^2 - \left(\frac{6.34}{12.4}\right)^2 (0.552)^2\right]^{1/2} = 0.266$$

$$\left(\frac{V}{V_p}\right)_1 = 0.060 + 0.266 = 0.326$$

The above coordinates are plotted to form the approximate interaction diagram shown in Fig. 26 for $A_r = 0$.

There are no positions along the beam where the opening can be placed for the case where $A_r = 0$ since all points on the internal beam force curve lie outside the failure envelope as shown in Fig. 27a.

Opening Locations for $A_r$ Large Enough to Accommodate Maximum Beam Shear

To determine the reinforcing area required to reach the maximum beam shear, a trial and error process is used since the equations for eccentric web openings become quite unwieldy when the $A_r$ term is isolated.

A brief examination of Fig. 26 will show that the $V/V_p$ values for the shear spans are a fairly large distance from the vertical leg of the interaction diagram for $A_r = 0$. This indicates that a relatively large area of reinforcement is required to include these points in the failure envelope.

After some preliminary trials, Try $A_r = 1.88\ in^2$

| Use 1-Bar 3 x 5/8 above and below the opening on one side only. |
|---|

($A_r = 1.88\ in^2$ ; $b_r/t_r = 4.8 < 8.5$)

Calculation of interaction diagram coordinates using formulas presented in Appendix IV with $A_r = 1.88\ in^2$, e = 3 in.:

$$\beta_T = -\frac{(2)(0.157)}{1.157}\left(\frac{1.88}{6.34}\right) + \frac{12.4}{(2)(6.34)}\left[\left(1 - \frac{12+6}{26.69}\right)^2 \frac{1}{1.157} - \frac{(16)(0.157)(1.88)^2}{(1.157)^2(12.4)^2}\right]^{1/2} = 0.135$$

$$\beta_B = -\frac{(2)(0.889)}{1.889}\left(\frac{1.88}{6.34}\right) + \frac{12.4}{(2)(6.34)}\left[\left(1 - \frac{12-6}{26.69}\right)^2 \frac{1}{1.889} - \frac{16(0.889)}{(1.889)^2}\left(\frac{1.88}{12.4}\right)^2\right]^{1/2} = 0.186$$

$$\left(\frac{M}{M_p}\right)_0 = \frac{1 + \frac{1.88}{6.34}\left(\frac{12}{26.69}\right) + \frac{12.4}{6.34}\left[\frac{1}{4} - \frac{(6)^2 + (2)(6)(3) - (3)^2}{(26.69)^2} - \frac{(0.463)(3)^2}{(3.463)(26.69)^2}\right]}{1 + \frac{12.4}{(4)(6.34)}}$$

$$= 0.971$$

$$\left(\frac{M}{M_p}\right)_1 = \frac{1 - \frac{1.88}{6.34} - 0.186}{1 + \frac{12.4}{(4)(6.34)}} = 0.348$$

$$\left(\frac{V_T}{V_p}\right)_1 = \left[\left(\frac{1}{2} - \frac{6 + 3}{26.69}\right)^2 - \left(\frac{6.34}{12.4}\right)^2 (0.135)^2\right]^{1/2} = 0.147$$

$$\left(\frac{V_B}{V_p}\right)_1 = \left[\left(\frac{1}{2} - \frac{6 - 3}{26.69}\right)^2 - \left(\frac{6.34}{12.4}\right)^2 (0.186)^2\right]^{1/2} = 0.376$$

$$\left(\frac{V}{V_p}\right)_1 = 0.147 + 0.376 = 0.523$$

$(V/V_p)_1$ is greater than the maximum $V/V_p$ ratio in the girders (0.522), therefore the trial $A_r$ is okay.

The above coordinates are plotted in Fig. 26 to describe the interaction diagram for $A_r = 1.88\ in^2$. It should be noted that while the maximum shear alone and shear along with low moment are within the failure envelope, as the moment increases some regions of the girder cannot accommodate the opening as shown in Fig. 27b.

Opening locations for $(A_r)_{min}$

$$(A_r)_{min} = \frac{(9.5)(0.463)}{\sqrt{3}} = 2.54\ in^2$$

| Use 1-Bar 3-1/2 x 3/4 above and below the opening on one side only |
|---|

($A_r = 2.63\ in^2 > 2.54\ in^2$ ; $b_r/t_r = 4.7 < 8.5$)

Calculations of interaction diagram coordinates using formulas presented in Appendix IV with $A_r = 2.63\ in^2$, e = 3 in.:

$$\left(\frac{M}{M_p}\right)_0 = \frac{1 + \frac{2.63}{6.34}\left(\frac{12}{26.69}\right) + \frac{12.4}{6.34}\left[\frac{1}{4} - \frac{(6)^2 + (2)(6)(3) - (3)^2}{(26.69)^2} - \frac{(0.463)(3)^2}{(3.963)(26.69)^2}\right]}{1 + \frac{12.4}{(4)(6.34)}}$$

$$= 1.007$$

$$\left(\frac{M}{M_p}\right)_1 = \frac{1 - \frac{2.54}{6.34}}{1 + \frac{12.4}{(4)(6.34)}} = 0.403$$

Note that in the above calculation for $(M/M_p)_1$, the calculated value of $(A_r)_{min}$ was used in place of the reinforcing bar area. This is because $A_r$ is subtracted from one in the equation and logic tells us that more reinforcement must increase the load carrying capacity of a member, not decrease it. Therefore the $(A_r)_{min}$ value calculated as above should be used to prevent overly conservative results.

$$\left(\frac{V}{V_p}\right)_1 = 1 - \frac{12}{26.69} = 0.550$$

These coordinates are plotted in Fig. 26 to form the interaction diagram for $A_r = 2.63\ in^2$. With this area of reinforcement, the centerline of the opening can be up to 8.6 ft from the supports in the shear spans and anywhere in the center portion as shown in Fig. 27c.

If $A_r$ were increased above $(A_r)_{min}$, point 1 on the interaction diagram would move upward to include more points on the internal beam force curve. However, it would be uneconomical to try to include additional positions along the beam since little is gained for a significant increase in $A_r$.

## SUMMARY AND DESIGN DETAILS

The possible opening locations for the beams and girders are summarized in Figs. 24 and 27, respectively. The positions where openings can be placed are obtained graphically from Figs. 23 and 26, noting that where the internal beam forces fall inside the failure envelope, an opening can be placed. On the interaction diagram for the floor beams, Fig. 23, it can be seen that if $A_r$ were reduced from $(A_r)_{min}$ the sloping portion of the diagram could be brought closer to the internal beam forces. Conversely, in Fig. 26, the interaction diagram for the girders, a substantial increase in $A_r$ over $(A_r)_{min}$ would provide a very minor expansion in the possible locations of the opening. In general, when concentrated loads are involved it would be difficult as well as uneconomical to provide sufficient reinforcement to allow positioning the opening at any desired location along the beam. Further restrictions are placed on opening locations in the girders due to limited experimental data on web crippling in beams with web openings in the vicinity of concentrated loads and reactions. It is therefore recommended that the edge of the opening be a distance of at least d/2 from the points where concentrated loads or reactions are introduced unless bearing stiffeners are provided [6].

The following suggestions for design details are provided to supplement the information presented in the design example:

1. Bars were used on one side of the web only.
    a. This gives approximately the same results as bars placed on both sides of the web [5].
    b. The reinforcement is cheaper to fabricate since welding is required on one side only.

2. The reinforcing bars should be checked for:

   a. Weld compatability with web.

   b. The $b_r/t_r$ ratio.

3. The reinforcing bars should be extended beyond the edge of the opening:

   a. a sufficient length to develop the strength of the bar in the welds.

   b. a minimum of 3 inches.

4. The welds should:

   a. be in accordance with the AISC Specifications.

   b. have a weld stress of 1.7 times the allowable weld stress or less.

## ACKNOWLEDGMENTS

Support for the research described in this report was provided by National Science Foundation Grant GK-35762 and the Department of Civil Engineering at Kansas State University. This support is gratefully acknowledged.

The author wishes to express sincere appreciation to Dr. Peter B. Cooper for serving as major professor. Without his ready assistance and able guidance this thesis would not have been possible.

# APPENDIX I - REFERENCES


1. Bower, J. E., "Ultimate Strength of Beams with Rectangular Holes," Journal of the Structural Division, ASCE, Vol. 94, No. ST6, Proc. Paper 5982, June 1968.

2. Redwood, R. G. and McCutcheon, J. O., "Beam Tests with Unreinforced Web Openings," Journal of the Structural Division, ASCE, Vol. 94, No. ST1, Proc. Paper 5706, January 1968.

3. Cooper, P. B. and Snell, R. R., "Tests on Beams with Reinforced Web Openings," Journal of the Structural Division, ASCE, Vol. 98, No. ST3, Proc. Paper 8791, March 1972.

4. Congdon, J. G. and Redwood, R. G., "Plastic Behavior of Beams with Reinforced Holes," Journal of the Structural Division, ASCE, Vol. 96, No. ST9, Proc. Paper 7561, September 1970.

5. Frost, R. W., "Behavior of Steel Beams with Eccentric Web Holes," Technical Report 46.019-400 (1), Applied Research Laboratory, United States Steel Corp., February 1973.

6. Subcommittee on Beams with Web Openings, "Suggested Design Guides for Beams with Web Holes," Journal of the Structural Division, ASCE, Vol. 97, No. ST11, Proc. Paper 8536, November 1971.

7. Bower, J. E., "Recommended Design Procedures for Beams with Web Openings," Engineering Journal, AISC, Vol. 8, No. 4, October, 1971.

8. Redwood, R. G., "Tables for Plastic Design of Beams with Rectangular Holes," Engineering Journal, AISC, Vol. 9, No. 1, January 1972.

9. "Manual of Steel Construction," 7th Edition, American Institute of Steel Construction, New York, 1970.

10. Wang, T. M., Snell, R. R., Cooper, P. B., "Strength of Beams with Eccentric Reinforced Holes," Journal of the Structural Division, ASCE, Vol. 101, No. ST9, Proc. Paper 11540, September, 1975.

11. McNew, J. L., "Experimental Tests of Beams with Eccentric Web Openings," Master's Thesis, Department of Civil Engineering, Kansas State University, September, 1975.

12. Ahmad, S. H., "Elastic Tests on Steel Beams with Eccentric Rectangular Web Openings," Master's Thesis, Department of Civil Engineering, Kansas State University, August 1975.

13. "Uniform Building Code," 1973 Edition, International Conference on Building Officials, Whittier, California, 1973.

# APPENDIX II -- NOTATION

| | |
|---|---|
| $A_f$ | Area of one flange - $b_f$ x $t_f$ |
| $A_r$ | Area of reinforcement above opening, also area of reinforcement below opening |
| $(A_r)_{min}$ | Minimum area of reinforcement required to reach shear capacity of section |
| $A_v$ | Shear area - w x d-(PART I) |
| $A_w$ | Area of web - $t_x$ x d-(PART II) |
| M | Moment at centerline of opening |
| $M_p$ | Plastic moment of section - $F_y$ x Z |
| $M_u$ | Moment at centerline of opening at ultimate load |
| $\left\lvert\frac{M}{M_p}\right\rvert_x$ | Absolute value of moment to plastic moment ratio along beams and girders |
| $\left(\frac{M}{M_p}\right)_0$, $\left(\frac{M}{M_p}\right)_1$ | Coordinates of Points on approximate interaction diagram |
| P | Concentrated load |
| $P_u^{Cor}$ | Experimental ultimate load corrected for strain hardening |
| $P_u^{Exp}$ | Experimental ultimate load |
| $P_u^{Theo}$ | Theoretical ultimate load |
| V | Shear force at centerline of opening |
| $V_p$ | Plastic shear capacity of section |
| $V_u$ | Shear force at centerline of opening at ultimate load |
| $\left\lvert\frac{V}{V_p}\right\rvert_x$ | Absolute value of shear force to plastic shear capacity along beams and girders |
| $\left(\frac{V}{V_p}\right)_1$ | Coordinate of point on approximate interaction diagram $\left(\frac{V_B}{V_p}\right)_1 + \left(\frac{V_T}{V_p}\right)_1$ |

| | |
|---|---|
| $\left(\frac{V_B}{V_p}\right)_1$ | Ratio of shear force in bottom tee section ($V_B$) to plastic shear capacity for point 1 on approximate interaction diagram |
| $\left(\frac{V_T}{V_p}\right)_1$ | Ratio of shear force in top tee section ($V_T$) to plastic shear capacity for point 1 on approximate interaction diagram |
| X | Distance between centerline of opening and centerline of beam - (PART I) |
| Z | Plastic section modulus |
| a | One-half opening length |
| b | Flange width - (PART I) |
| $b_f$ | Flange width - (PART II) |
| $b_r$ | Width of reinforcement |
| c | Web thickness plus width of reinforcement - $b_r + t_w$ |
| d | Section depth |
| e | Eccentricity-distance between mid-depth of section and mid-depth of opening |
| h | One-half opening depth |
| r | Radius of opening corners |
| t | Flange thickness - (PART I) |
| $t_f$ | Flange thickness - (PART II) |
| $t_r$ | Thickness of reinforcment |
| $t_w$ | Web thickness - (PART II) |
| u | Distance from edge of opening to face of reinforcement |
| w | Web thickness - (PART I) |
| w | Uniformly distributed load - (PART II) |
| x | Coordinate defining positions along beams and girders - (PART II) |
| $\alpha,\beta$ | Coefficients used in approximate design formulas with subscripts T and B to denote top and bottom tee sections, respectively. |

# APPENDIX III - SAMPLE CALCULATIONS

## Design of Test Specimen - Beam 5

1. From tensile coupon tests, average $F_y$ = 40.80 ksi

2. From measured beam dimensions, average

| | | Nominal |
|---|---|---|
| d = | 16.09" | (16.00) |
| b = | 7.002" | (7.000) |
| t = | 0.472" | (0.503) |
| w = | 0.335" | (0.307) |

3. $Z = bt(d-t) + \frac{1}{4} w(d-2t)^2$

Using nominal dimensions:

$$Z_{nom.} = (7.000)(0.503)(16.00-0.503) + (\tfrac{1}{4})(0.307)[16.00-(2)(0.503)]^2$$

$$Z_{nom} = 71.82 \text{ in.}^3$$

From AISC Manual of Steel Construction:

$$Z_{hnbk} = 72.8 \text{ in.}^3$$

$Z_{hnbk} - Z_{nom} = 72.8 - 71.82 \simeq 1.0 \text{ in.}^3$ ← Attribute to contribution of flange-web fillets - add to Z computed from measured dimensions.

Using measured dimensions:

$$Z_{meas} = (7.002)(0.472)(16.09-0.472) + (\tfrac{1}{4})(0.335)[16.09-(2)(0.472)]^2$$

$Z_{meas} = 70.83 \text{ in.}^3$ ← Add $1.0 \text{ in.}^3$ for flange-web fillets.

$$\boxed{\text{Use } Z = 71.83 \text{ in.}^3}$$

4. $V_p = w(d-2t)\ F_y/\sqrt{3} = A_v F_y/\sqrt{3}$

$$(A_v)_{meas} = (0.335)[16.09-(2)(0.472)] = 5.07 \text{ in.}^2$$

5. M/V = 30 in., Let $V/V_p = 0.6 \rightarrow M = 0.6(30)\ V_p = 18\ V_p$

$$M/M_p = 18V_p/M_p = 18A_v F_y/\sqrt{3}\, ZF_y = 18A_v/\sqrt{3}\, Z$$

$$M/M_p = (18)(5.07)/\sqrt{3}\ (71.83) = 0.734$$

Coordinates of Ray on Interaction Diagram

$$\boxed{V/V_p = 0.6,\ M/M_p = 0.734}$$

6. Moment at the center of the opening with a plastic hinge at midspan.

$$M_{\text{℄ Beam}} = M_p$$

$$M = \frac{30}{55} M_p = 0.545\ M_p$$

$$M/M_p = 0.545 \qquad \text{for failure at midspan}$$

In the interaction diagram below the intersection of the curve and the horizontal, dotted line labeled "No Cover Plates" is clearly below the intersection of the curve and the ray representing the moment-to-shear ratio of 30". This indicates that failure will occur due to the formation of a plastic hinge at midspan before the 4-hinge opening failure mechanism can form. Therefore, cover plates are required to obtain an opening failure.

7. 1-PL 5/16 x 4 is provided both top and bottom at midspan.

$$Z_{cpl} = 71.83 + (5/16)(4)(16.09 + 5/16) = 92.33 \text{ in.}^3$$

The plastic moment at the opening is still $M_p$ described above in 6. The plastic moment at midspan is now $M_{pcp}$ ($M_p$ with cover plates). For the failure to take place at midspan, the moment at the center of the opening would be:

$$M = 0.545\ M_p \frac{M_{pcp}}{M_p}$$

$$M/M_p = 0.545\ M_{pcp}/M_\Gamma = 0.545\ \frac{92.33}{71.83} = 0.701$$

From the interaction diagram below it is clear that the intersection of the dotted line marked "Cover Plates" and the curve is above the intersection representing opening failure. The failure of the opening should therefore take place before a plastic hinge can form at midspan.

8. The $M/M_p$ ratio at the point representing opening failure is approximately 0.658.

$$M_u = 0.658\ M_p = 0.658\ ZF_y = (0.658)(71.83(40.80) = 1928 \text{ in.-kips}$$

$$\frac{P_u}{2} \times 30 = M_u \rightarrow P_u = \frac{M_u}{15} = \frac{1928}{15} = 128.6 \text{ kips (For opening failure)}$$

$$P_u^{Theo} \simeq 129 \text{ kips}$$

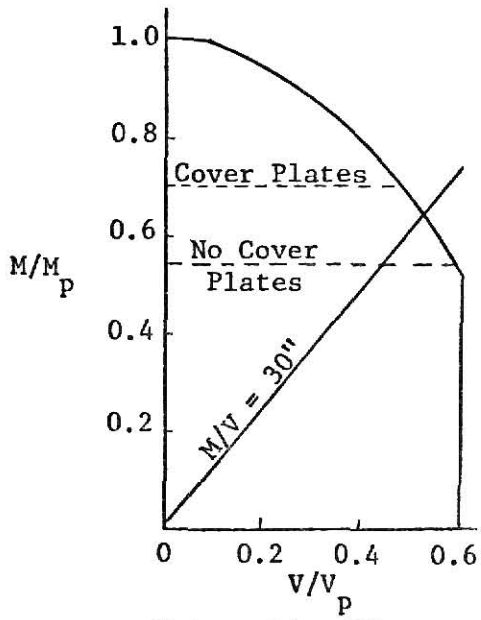


Interaction Diagram--Beam 5

## APPENDIX IV - APPROXIMATE INTERACTION DIAGRAM EQUATIONS

The equations presented below are used to construct an approximate interaction diagram similar to the one shown below [10]. Point zero on the diagram has the coordinates $[0,(M/M_p)_0]$, Point One is described by $[(V/V_p)_1, (M/M_p)_1]$, and the point on the $V/V_p$-axis is $(V/V_p)_1$ from the origin. These equations are for the general case of a reinforced eccentric web openings. To obtain equations for other, less general cases, $A_r$, e, or both $A_r$ and e are taken equal to zero as appropriate.

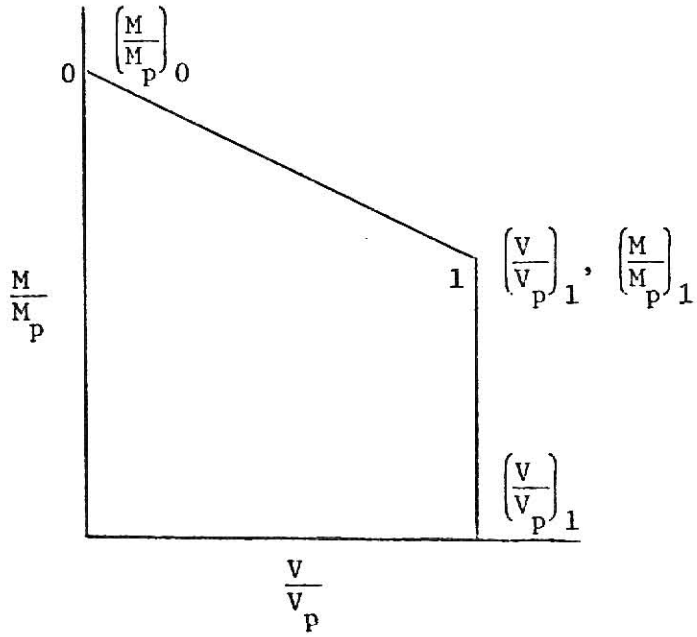


For $e \leq u$:

$$\left(\frac{M}{M_p}\right)_0 = \frac{1 + \frac{A_r}{A_f}\left(\frac{2h}{d}\right) + \frac{A_w}{A_f}\left(\frac{1}{4} - \frac{h^2 + 2he}{d^2}\right)}{1 + \frac{A_w}{4A_f}}$$

For $u \leq e \leq u + q + \frac{A_r}{t_w}$:

$$\left(\frac{M}{M_p}\right)_0 = \frac{1 + \frac{A_r}{A_f}\left(\frac{2h}{d}\right) + \frac{A_w}{A_f}\left(\frac{1}{4} - \frac{h^2 + 2he - e^2}{d^2} - \frac{t_w e^2}{cd^2}\right)}{1 + \frac{A_w}{4A_f}}$$

For $e \geq u + q + \frac{A_r}{t_w}$:

$$\left(\frac{M}{M_p}\right)_0 = \frac{1 + \frac{A_r}{A_f}\left(\frac{2h + 2e}{d} - \frac{A_r}{A_w}\right) + \frac{A_w}{A_f}\left(\frac{1}{4} - \frac{h^2 + 2he}{d^2}\right)}{1 + \frac{A_w}{4A_f}}$$

$$(A_r)_{min} = \frac{at_w}{\sqrt{3}}$$

For $A_r < (A_r)_{min}$:

$$\left(\frac{M}{M_p}\right)_1 = \frac{1 - \frac{A_r}{A_f} - \beta_B}{1 + \frac{A_w}{4A_f}}$$

$$\left(\frac{V}{V_p}\right)_1 = \left(\frac{V_T}{V_p}\right)_1 + \left(\frac{V_B}{V_p}\right)_1$$

$$\left(\frac{V_T}{V_p}\right)_1^2 = \left(\frac{1}{2} - \frac{h+e}{d}\right)^2 - \left(\frac{A_f}{A_w}\beta_T\right)^2$$

$$\left(\frac{V_B}{V_p}\right)_1^2 = \left(\frac{1}{2} - \frac{h-e}{d}\right)^2 - \left(\frac{A_f}{A_w}\beta_B\right)^2$$

For $A_r \geq (A_r)_{min}$

$$\left(\frac{M}{M_p}\right)_1 = \frac{1 - \frac{A_r}{A_f}}{1 + \frac{A_w}{4A_f}}$$ where the $A_r$ value is $(A_r)_{min}$

$$\left(\frac{V}{V_p}\right)_1 = 1 - \frac{2h}{d}$$

$$\beta_T = -\frac{2\alpha_T}{1+\alpha_T}\left(\frac{A_r}{A_f}\right) + \frac{A_w}{2A_f}\left[\left(1 - \frac{2h + 2e}{d}\right)^2 \frac{1}{1+\alpha_T} - \frac{16\alpha_T}{(1+\alpha_T)^2}\left(\frac{A_r}{A_w}\right)^2\right]^{1/2}$$

$$\beta_B = -\frac{2\alpha_B}{1+\alpha_B}\left(\frac{A_r}{A_f}\right) + \frac{A_w}{2A_f}\left[\left(1 - \frac{2h - 2e}{d}\right)^2 \frac{1}{1+\alpha_B} - \frac{16\alpha_B}{(1+\alpha_B)^2}\left(\frac{A_r}{A_w}\right)^2\right]^{1/2}$$

$$\alpha_T = \frac{3}{16}\left(\frac{d}{a}\right)^2 \left(1 - \frac{2h}{d} - \frac{2e}{d}\right)^2$$

$$\alpha_B = \frac{3}{16}\left(\frac{d}{a}\right)^2 \left(1 - \frac{2h}{d} + \frac{2e}{d}\right)^2$$

| Beam | 1 | 2 | 5 | 6 | 7 |
|---|---|---|---|---|---|
| X | 24" | 24" | 25" | 26" | 26" |
| a | 4.5" | 4.5" | 6" | 8" | 6" |
| h | 3" | 3" | 3" | 4" | 4" |
| r | 3/4" | 3/4" | 17/32" | 1/2" | 1/2" |
| Reinforcing Bars | None | One Side | Both Sides | One Side | One Side |
| Cover Plates | None | PL 5/16x4x24 | PL 5/16x4x31 | None | None |

Table 1. Test Variables

| Section | W 16x45 | | | W 16x40 | |
|---|---|---|---|---|---|
| Beam | 1 | 2 | Nominal | 5, 6, & 7 | Nominal |
| d (in.) | 16.11 | 16.10 | 16.10 | 16.09 | 16.00 |
| b (in.) | 7.00 | 7.015 | 7.039 | 7.002 | 7.000 |
| t (in.) | 0.538 | 0.539 | 0.563 | 0.472 | 0.503 |
| w (in.) | 0.383 | 0.382 | 0.346 | 0.335 | 0.307 |

Table 2. Beam Dimensions

| Beam | 1 | 2 | 5, 6, & 7 |
|---|---|---|---|
| Average $F_y$ (ksi) | 43.17 | 42.79 | 40.80 |
| Maximum Deviation from Average $F_y$ (%) | 3.96 | 2.17 | 2.82 |
| $A_v$ ($in^2$) | 5.76 | 5.74 | 5.07 |
| Z ($in^3$) | 81.29 | 81.39 | 71.83 |
| $V_p$ (kips) | 143.3 | 141.6 | 119.5 |
| $M_p$ (kip-in) | 3509 | 3483 | 2931 |

Table 3. Reference Values for Test Beams

| Beam | 1 | 2 | 5 | 6 | 7 |
|---|---|---|---|---|---|
| $P_u^{Theo}$ (kips) | 129 | 152 | 129 | 83 | 96 |
| $P_u^{Exp}$ (kips) | 150.3 | 184.8 | 147.8 | 94.4 | 114.0 |
| $V_u/V_p$ for $P_u^{Exp}$ | 0.524 | 0.652 | 0.618 | 0.395 | 0.477 |
| $M_u/M_p$ for $P_u^{Exp}$ | 0.642 | 0.796 | 0.756 | 0.483 | 0.583 |
| $P_u^{cor}$ (kips) | 136 | 155 | 124 | 84 | 101 |
| $V_u/V_p$ for $P_u^{cor}$ | 0.474 | 0.547 | 0.519 | 0.351 | 0.422 |
| $M_u/M_p$ for $P_u^{cor}$ | 0.581 | 0.668 | 0.635 | 0.430 | 0.517 |
| $\frac{P_u^{cor}}{P_u^{Theo}}$ | 1.05 | 1.02 | 0.96 | 1.01 | 1.05 |

Table 4. Ultimate Loads and Interaction Diagram Coordinates

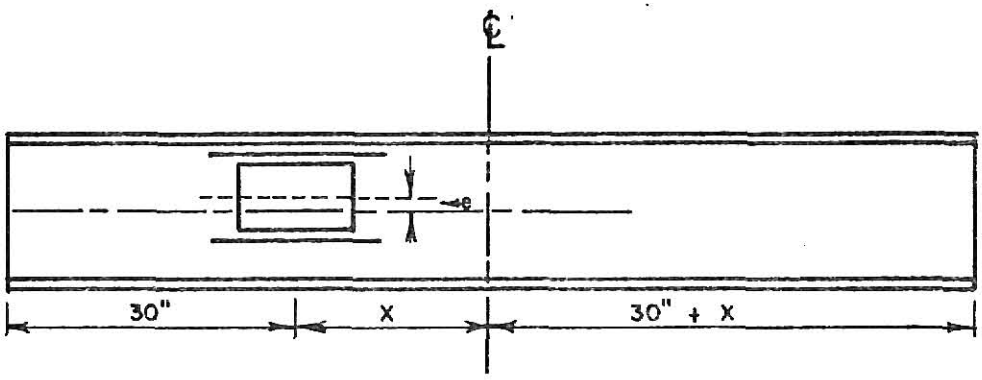


Figure 1a - Test Setup

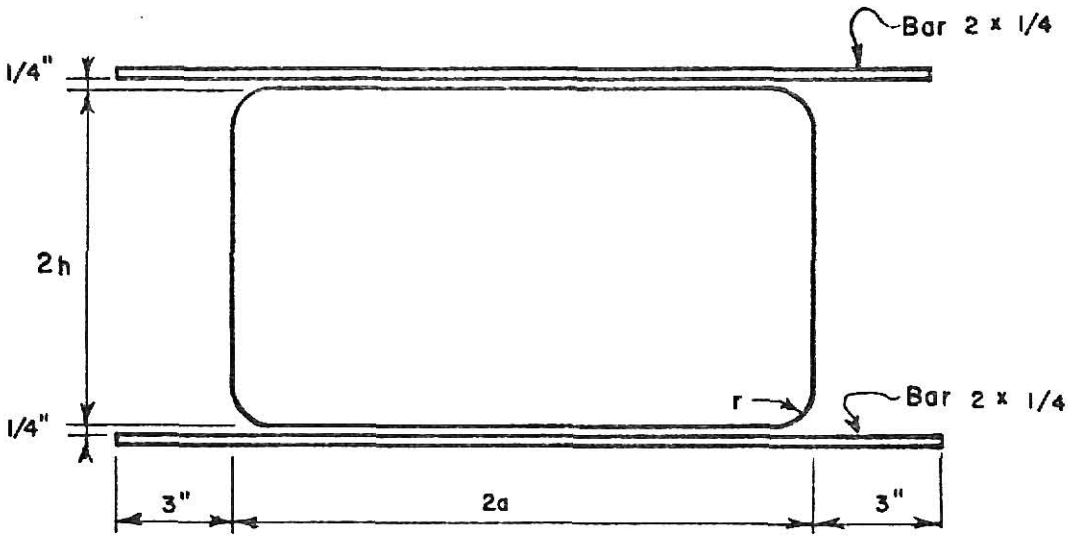


Figure 1b - Opening and Reinforcement Details

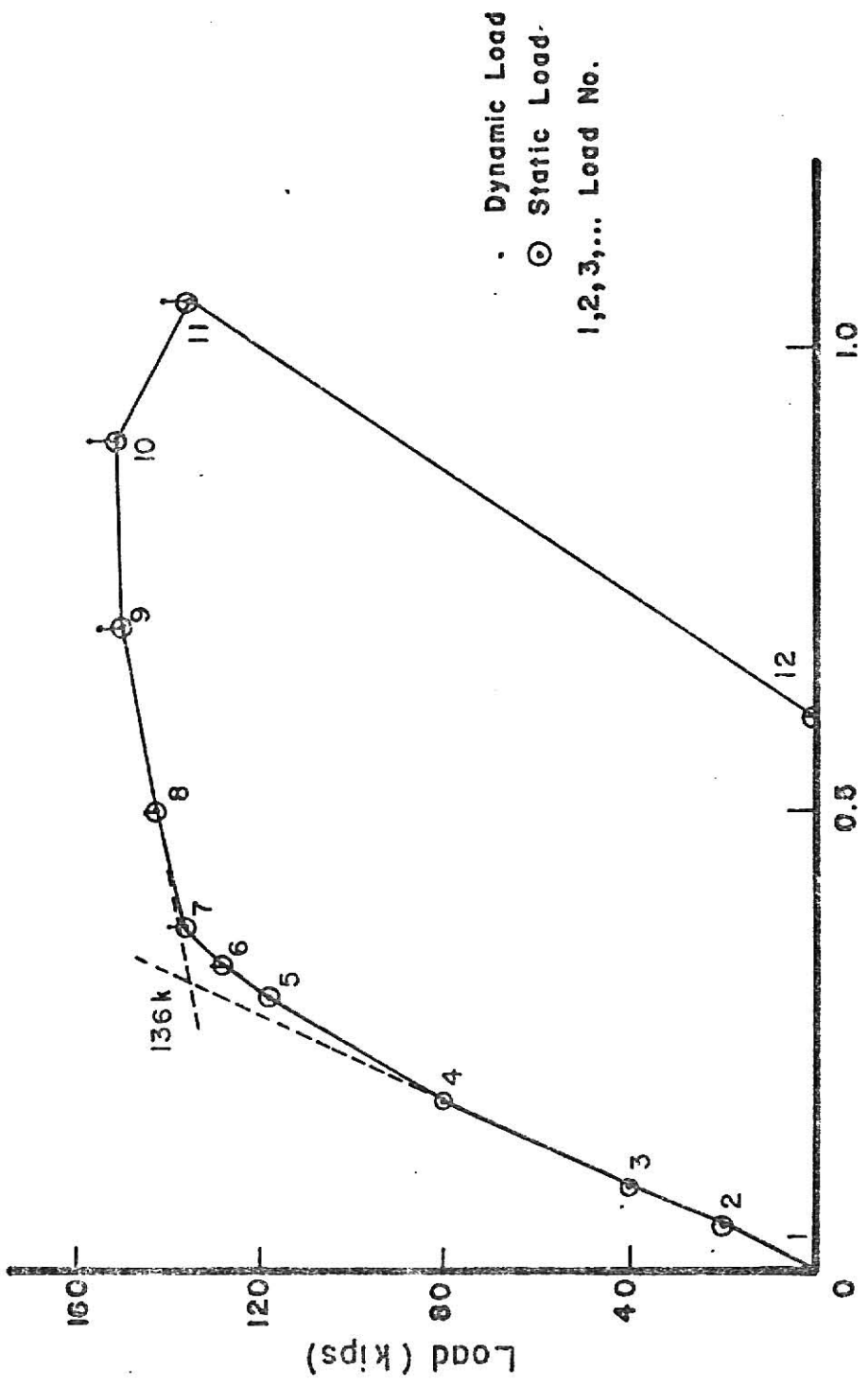


Figure 2 - Load Versus Midspan Deflection Curve--Beam 1

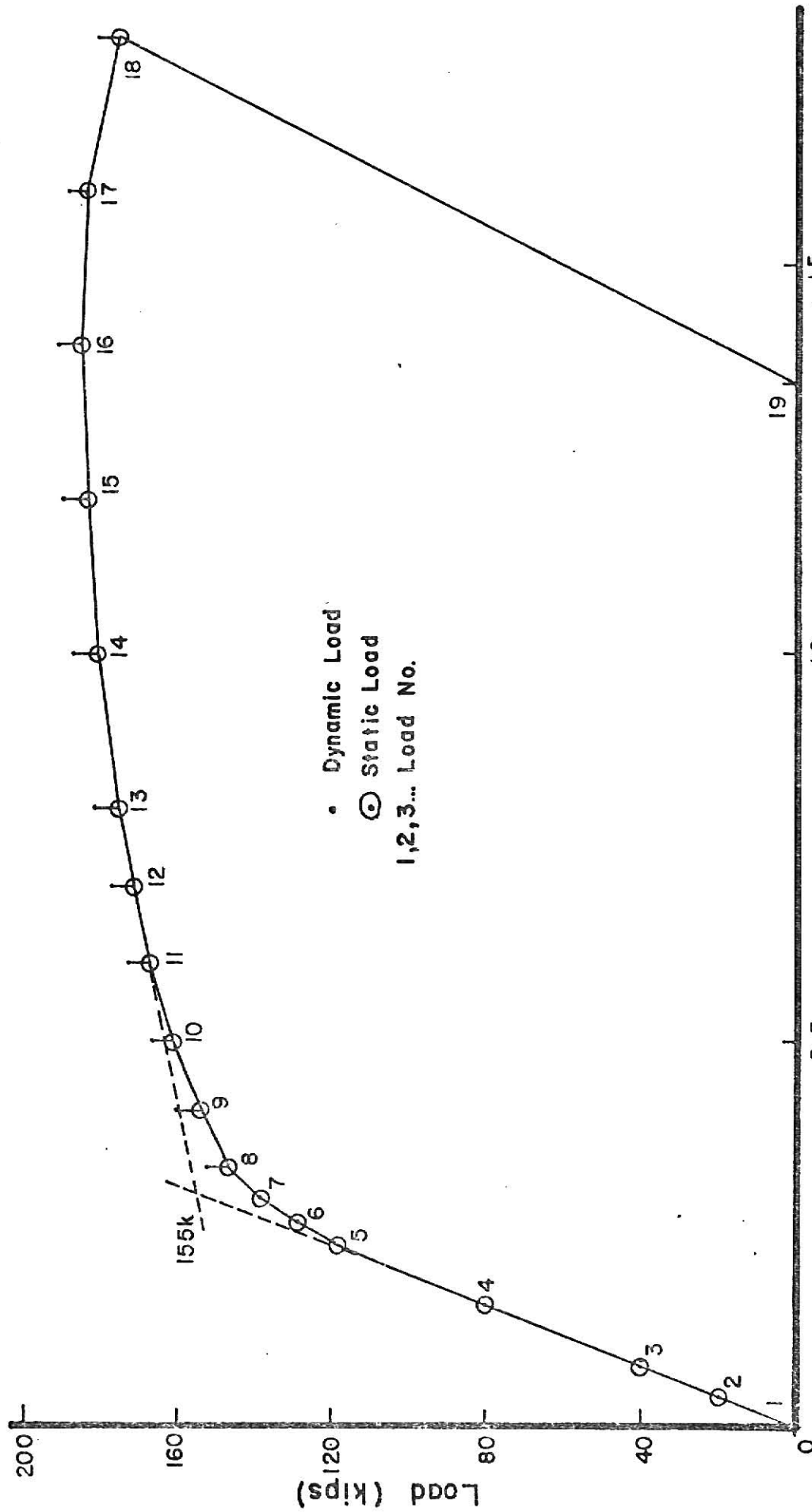


Figure 3 - Load Versus Midspan Deflection Curve--Beam 2

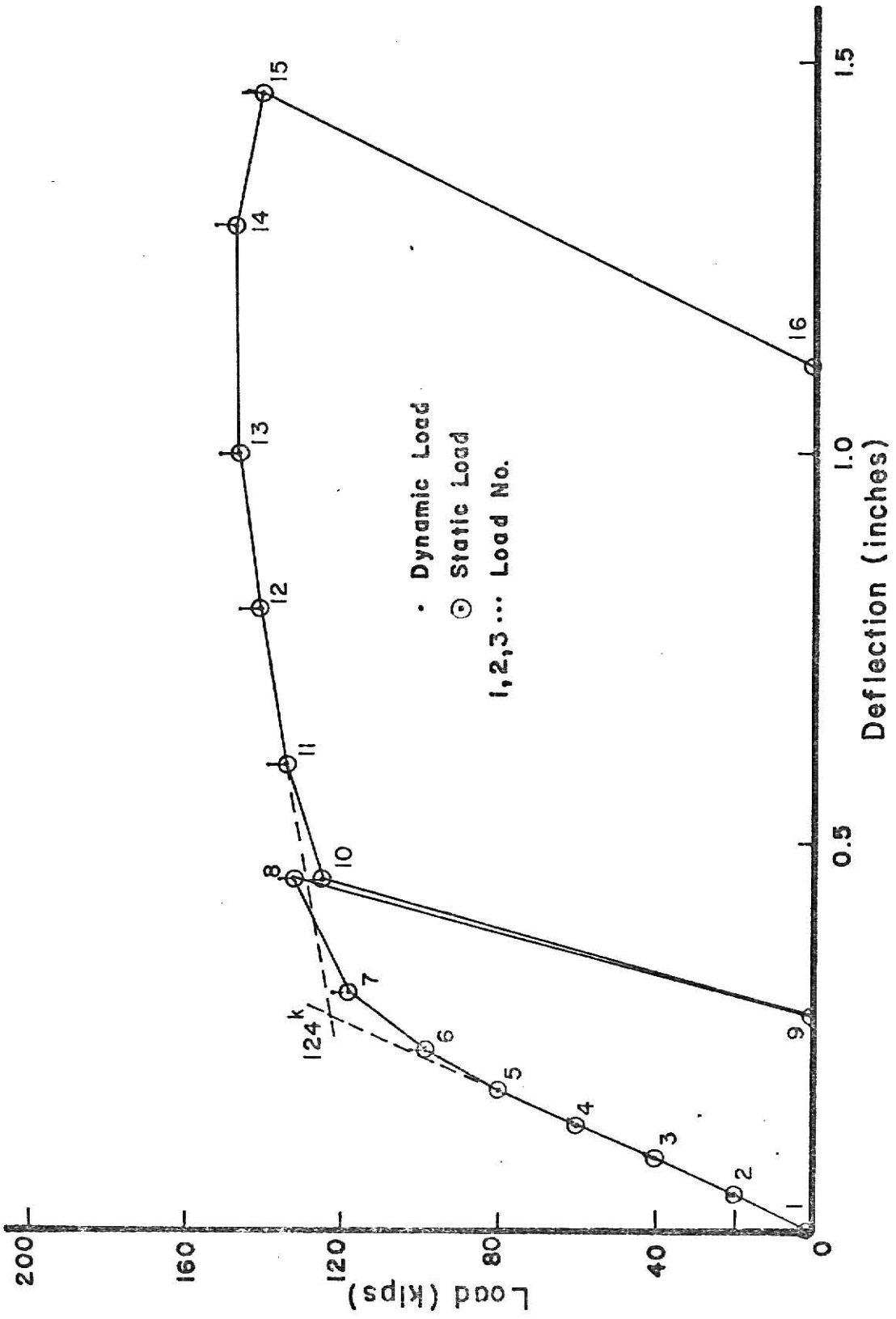


Figure 4 - Load Versus Midspan Deflection Curve--Beam 5

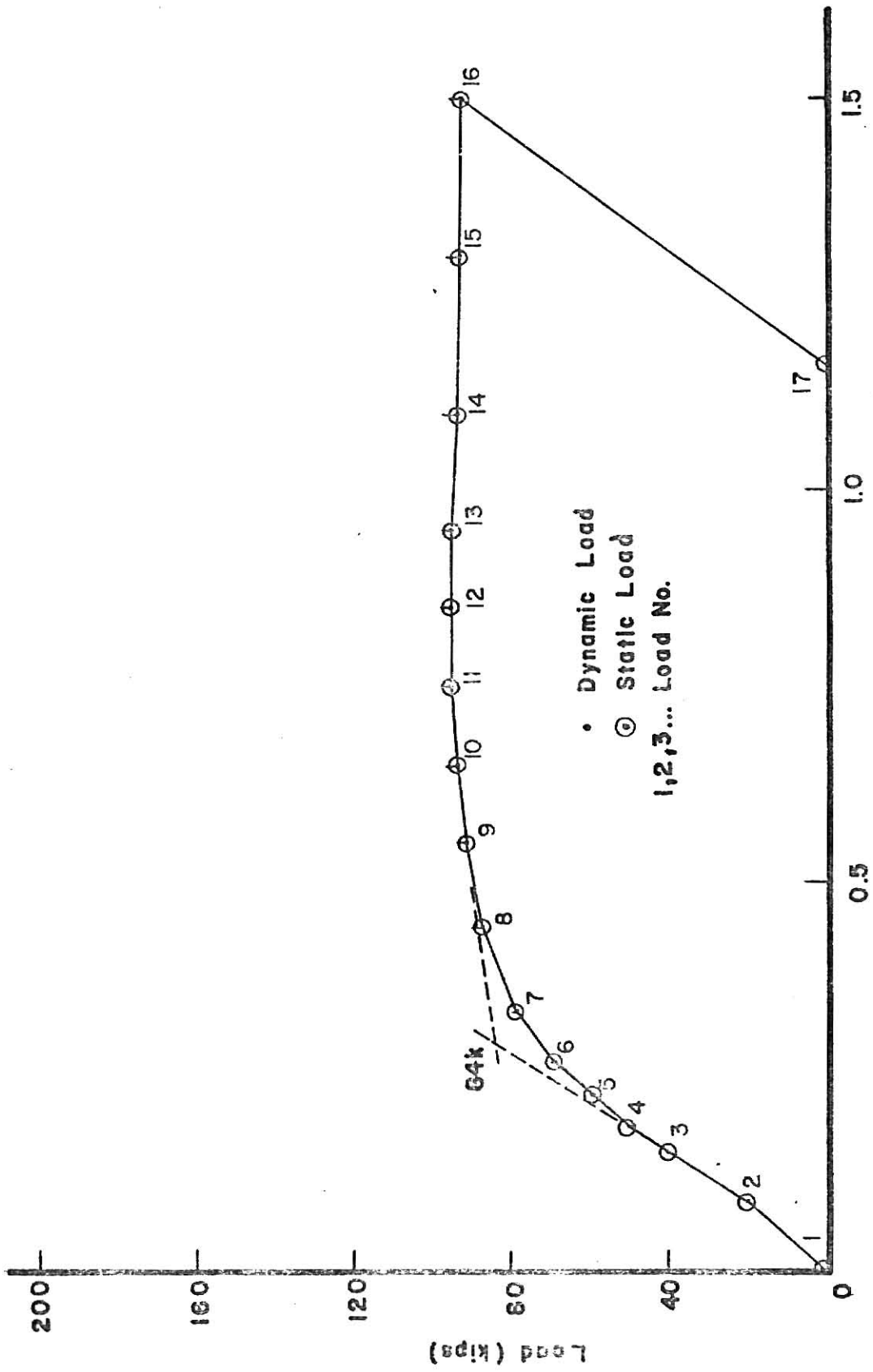


Figure 5 - Load Versus Midspan Deflection Curve--Beam 6

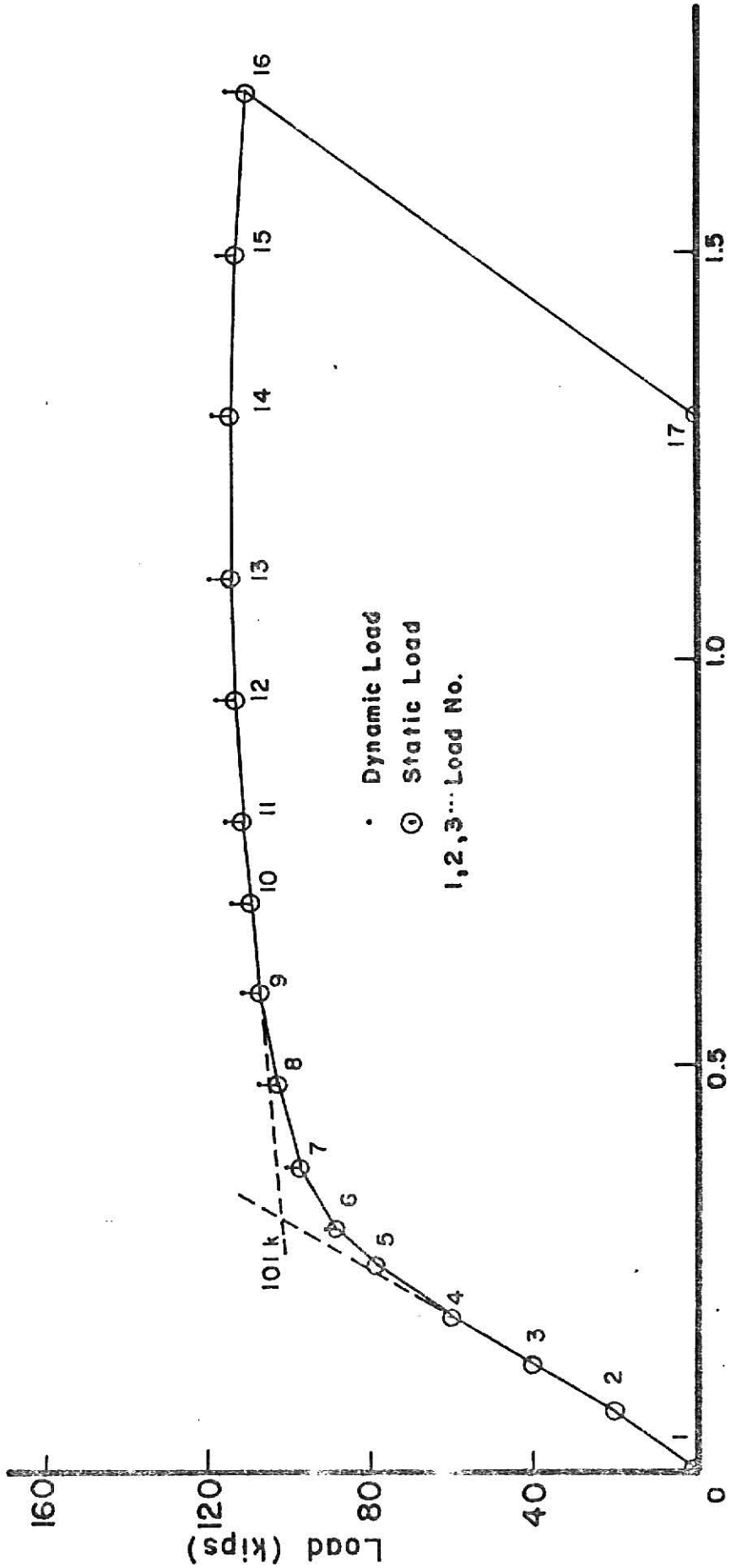


Figure 6 - Load Versus Midspan Deflection Curve--Beam 7

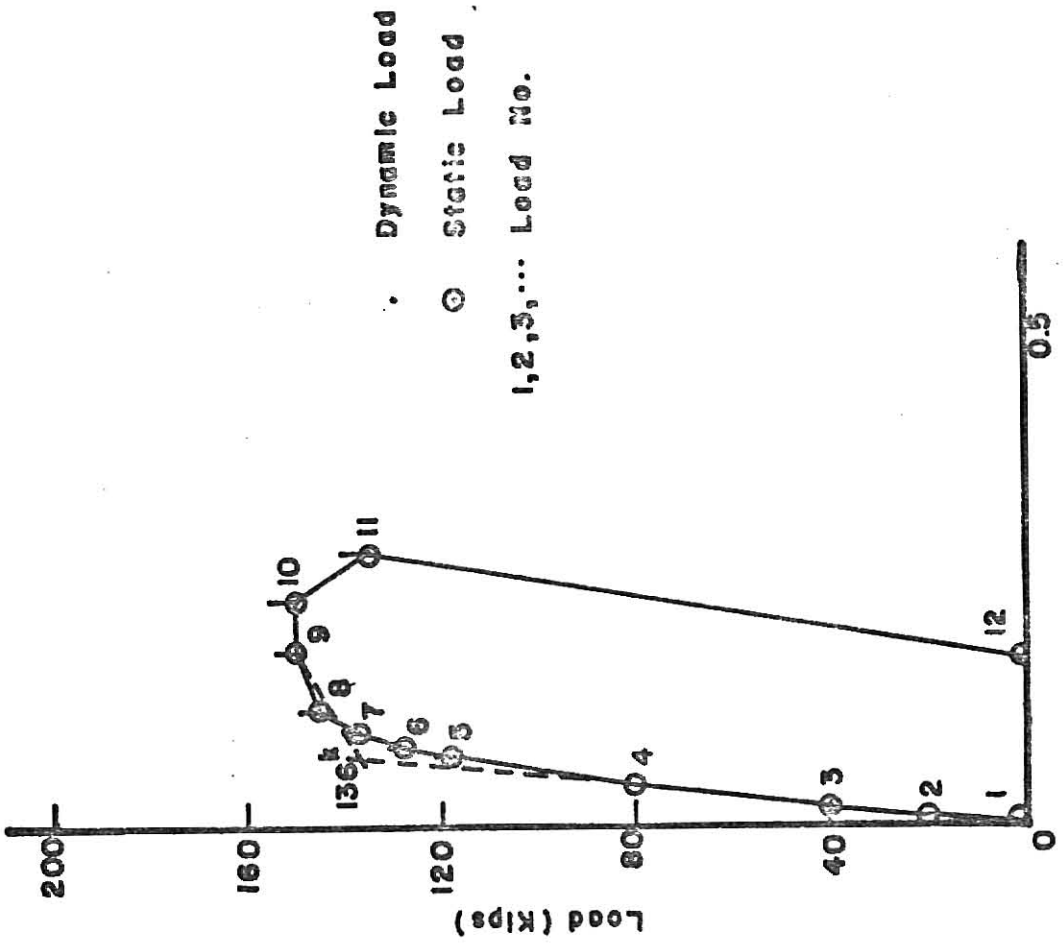


Figure 7 - Load Versus Relative Opening Deflection Curve--Beam 1

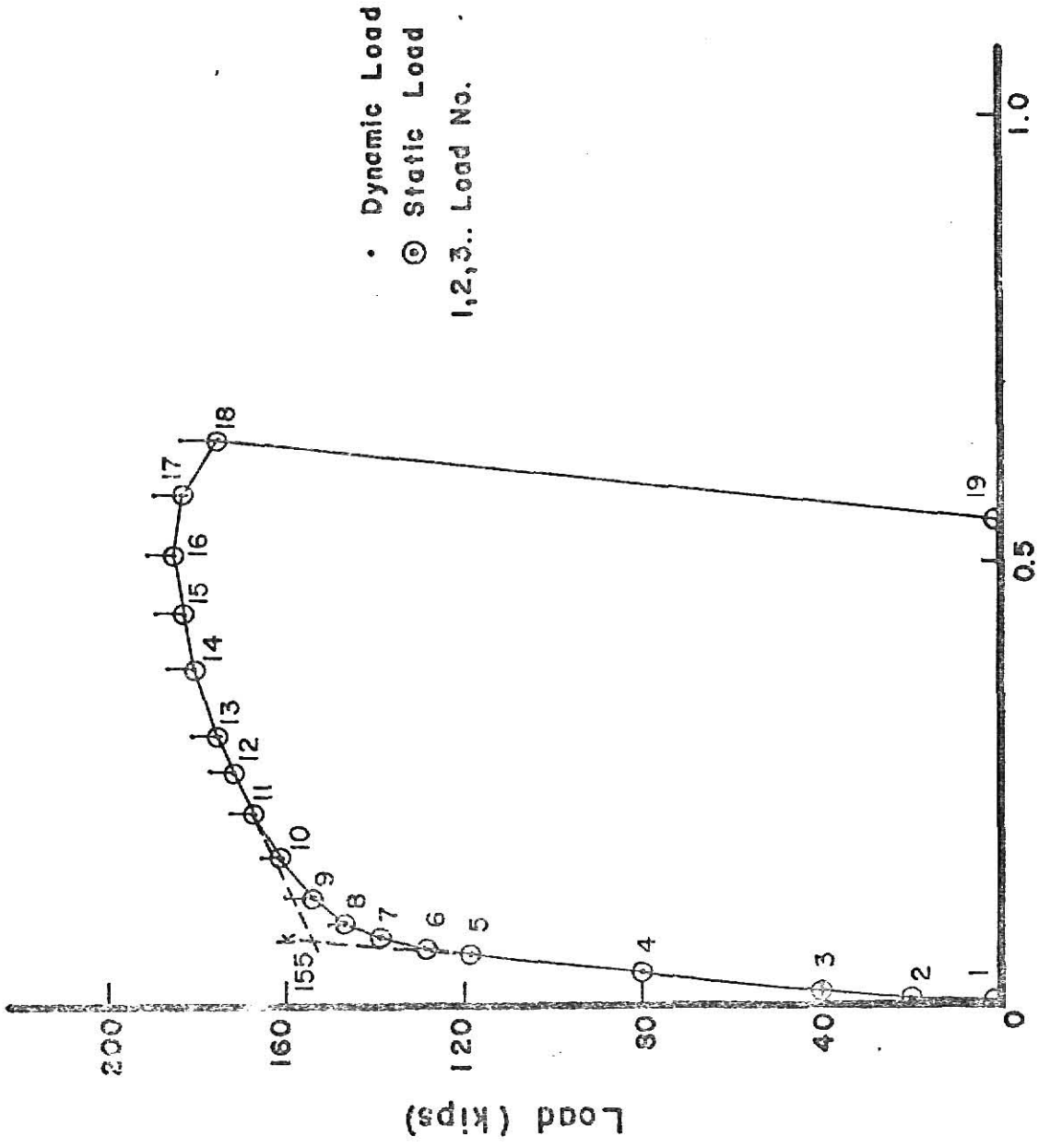


Figure 8 - Load Versus Relative Opening Deflection Curve--Beam 2

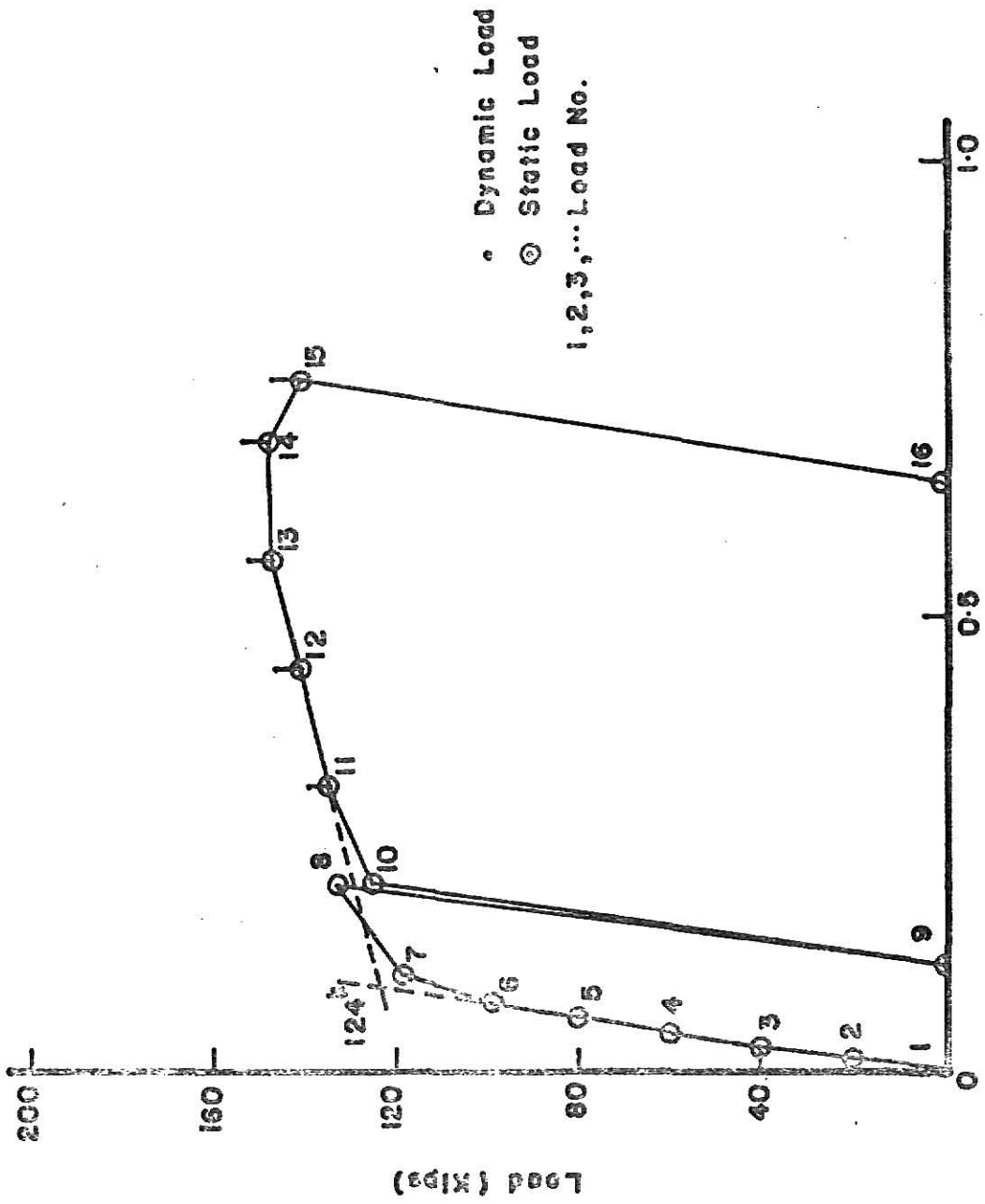


Figure 9 - Load Versus Relative Opening Deflection Curve--Beam 5

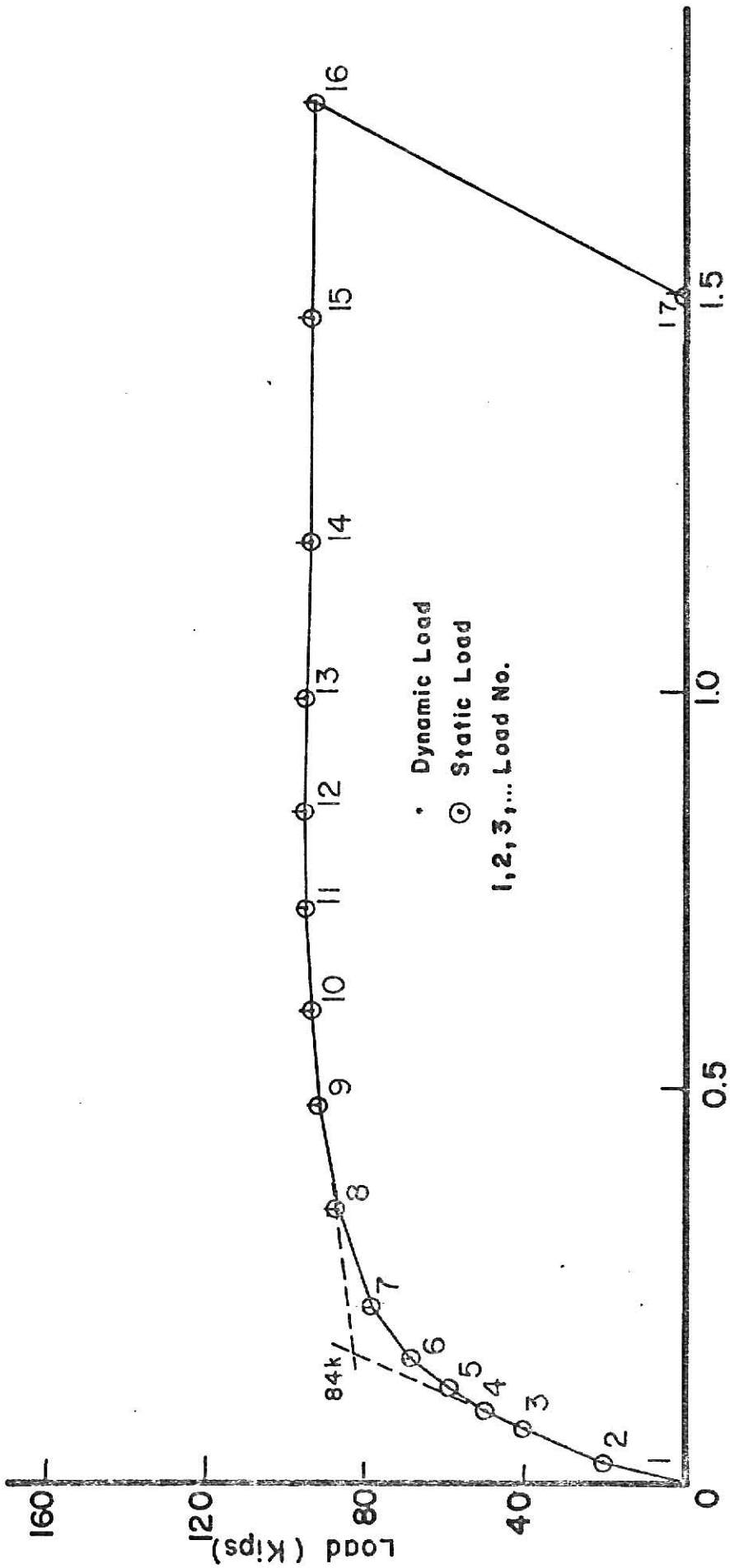


Figure 10 - Load Versus Relative Opening Deflection Curve--Beam 6

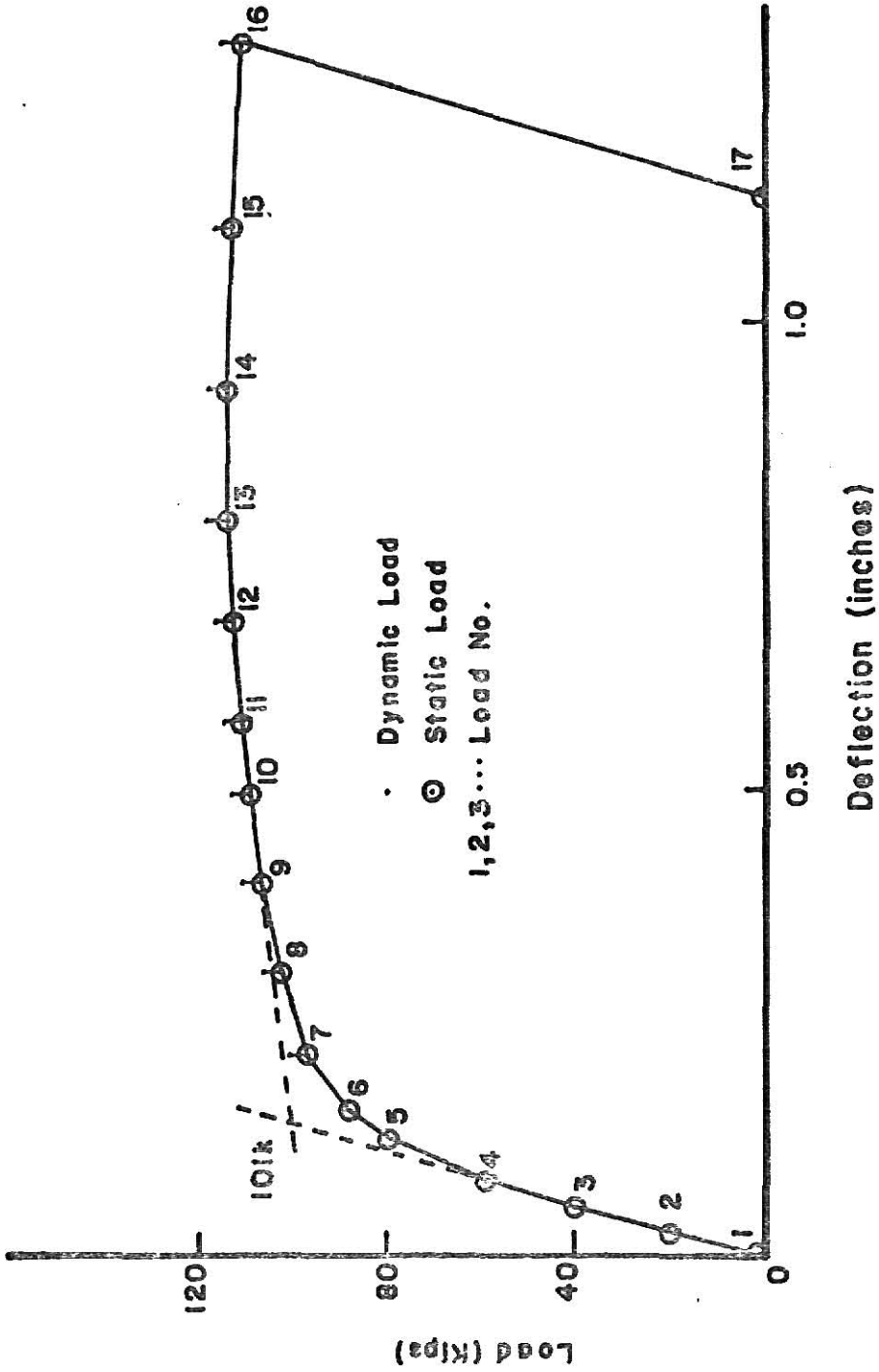


Figure 11 - Load Versus Relative Opening Defection Curve--Beam 7

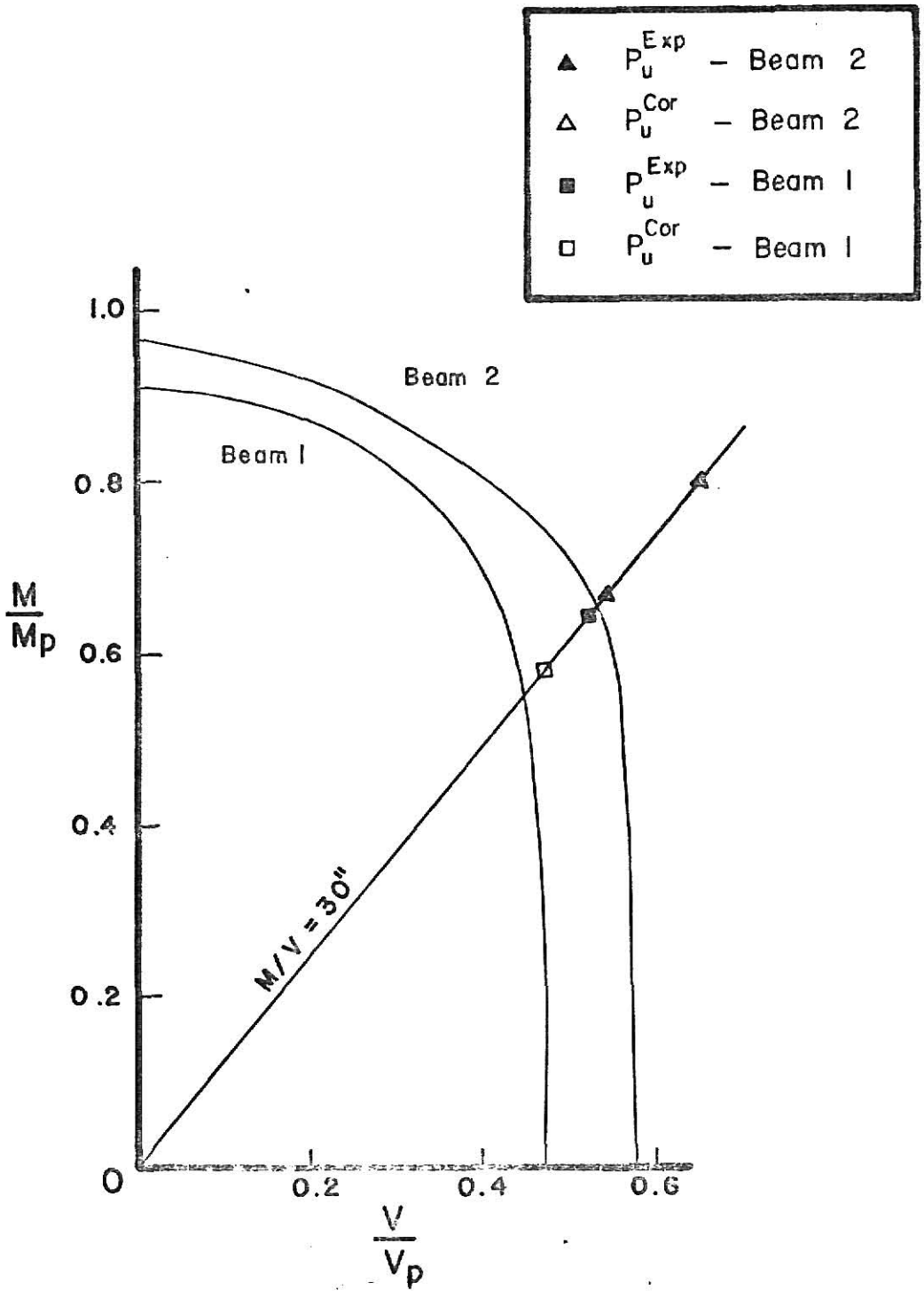


Figure 12 - Interaction Diagrams--Beams 1 & 2

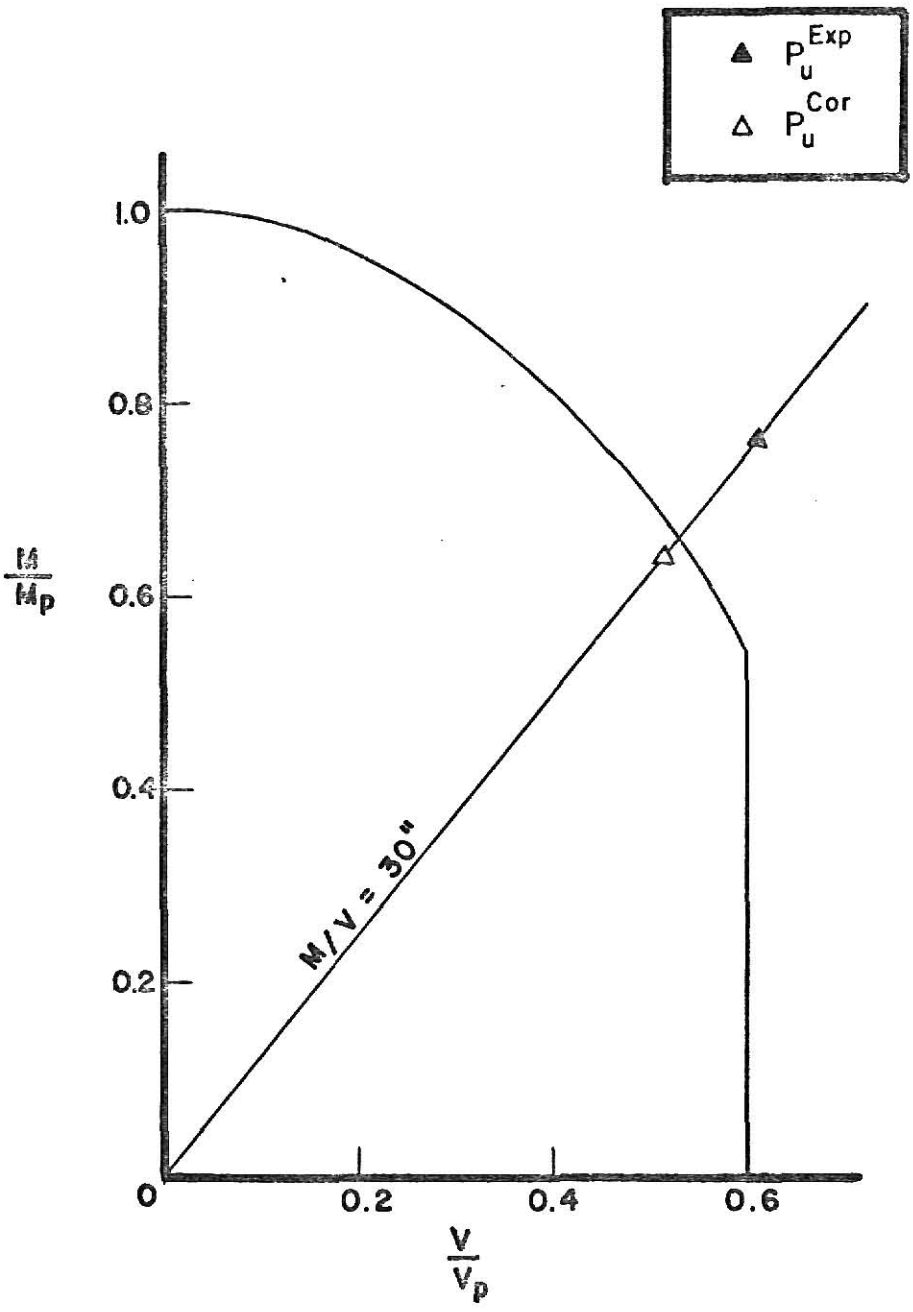


Figure 13 - Interaction Diagram--Beam 5

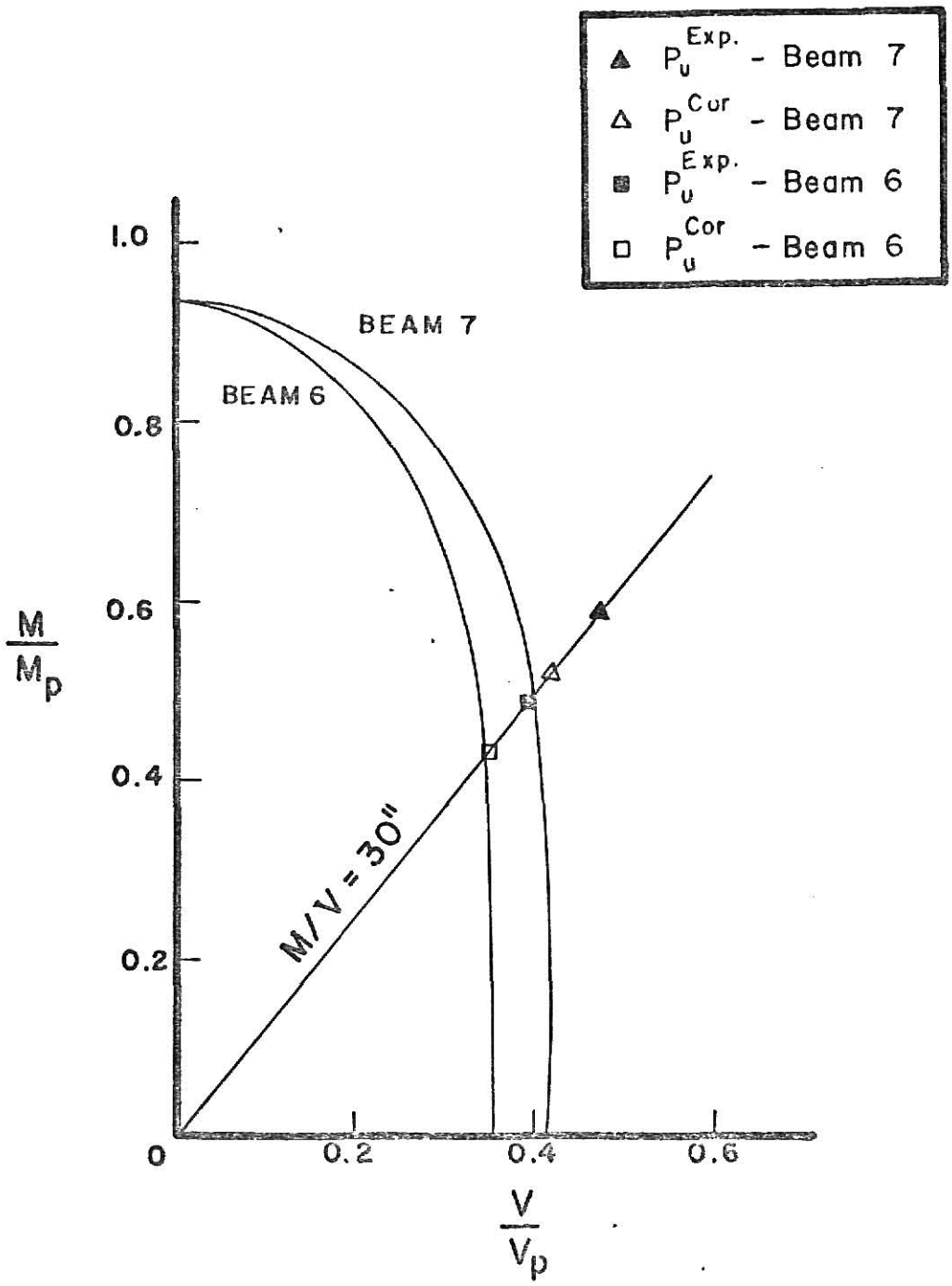


Figure 14 - Interaction Diagrams--Beams 6 & 7

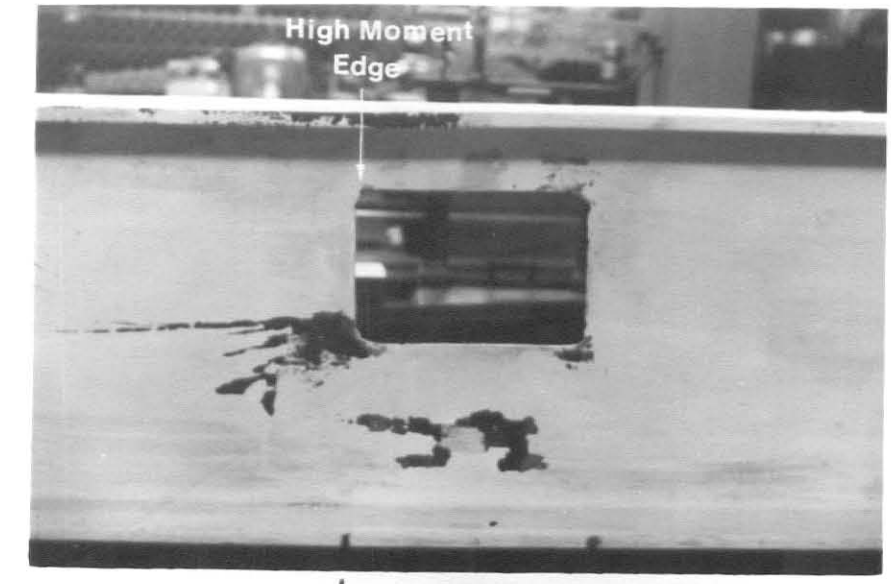


Figure 15a - Final Yield Pattern--Beam 1

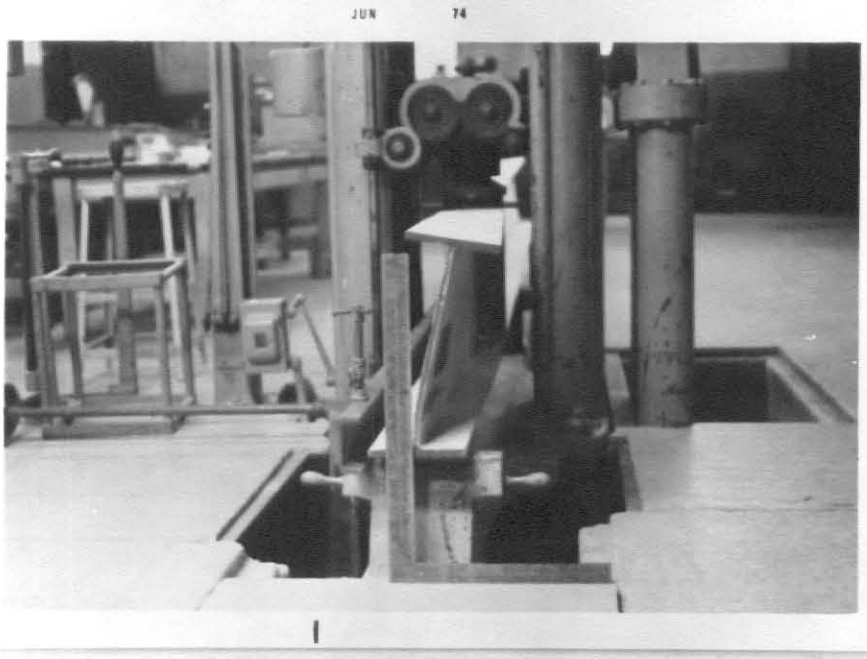


Figure 15b - Relative Displacement at Ultimate Load--Beam 1

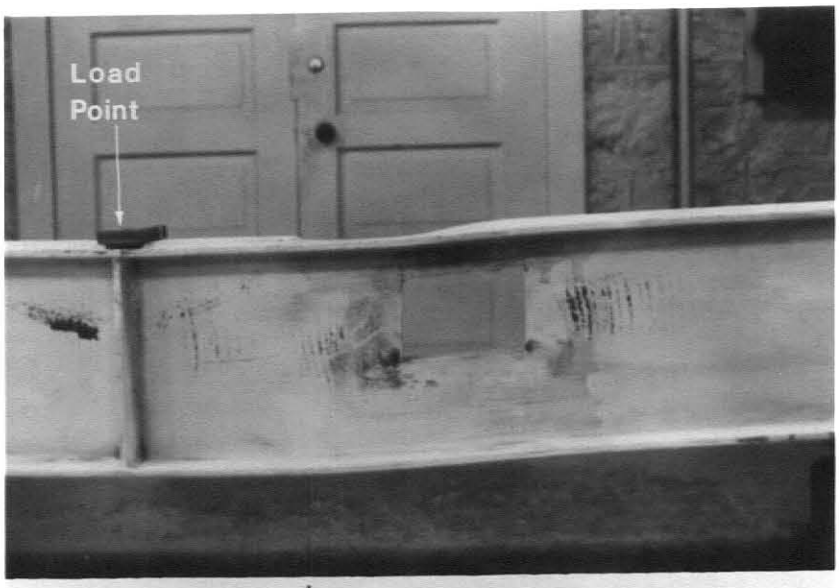


Figure 16a - Final Yield Pattern--Beam 2

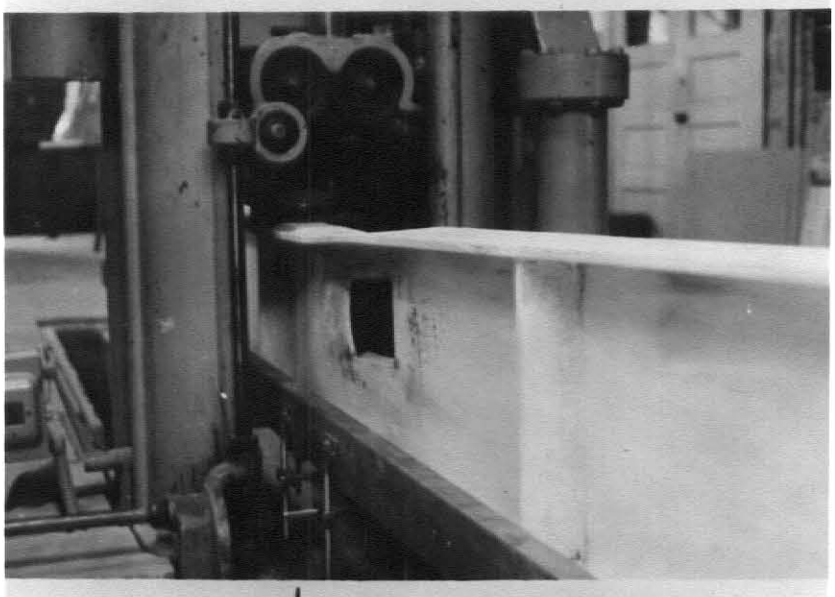

Figure 16b - Web Buckle at Ultimate Load--Beam 2

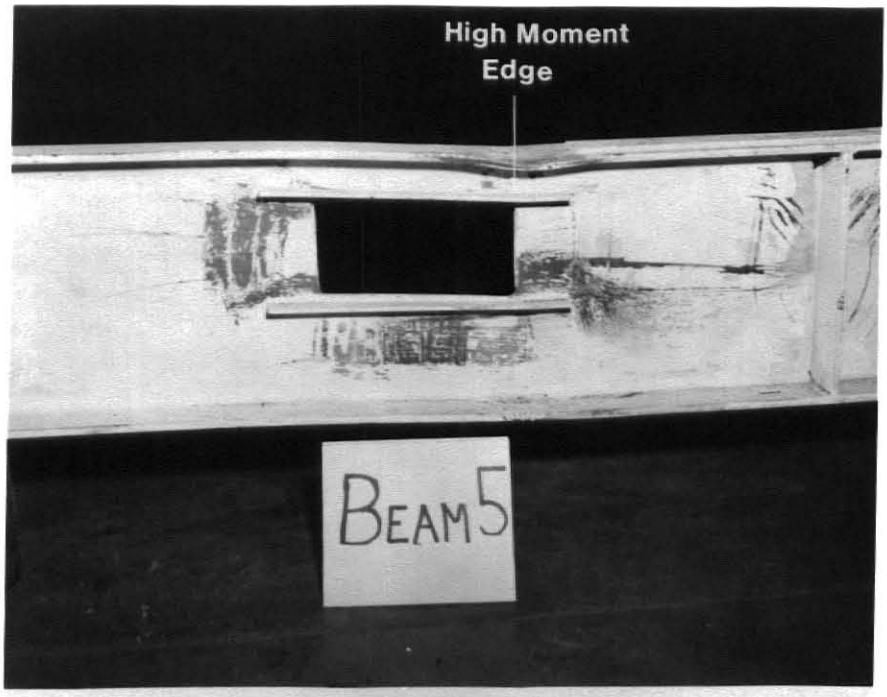


Figure 17 - Final Yield Pattern--Beam 5

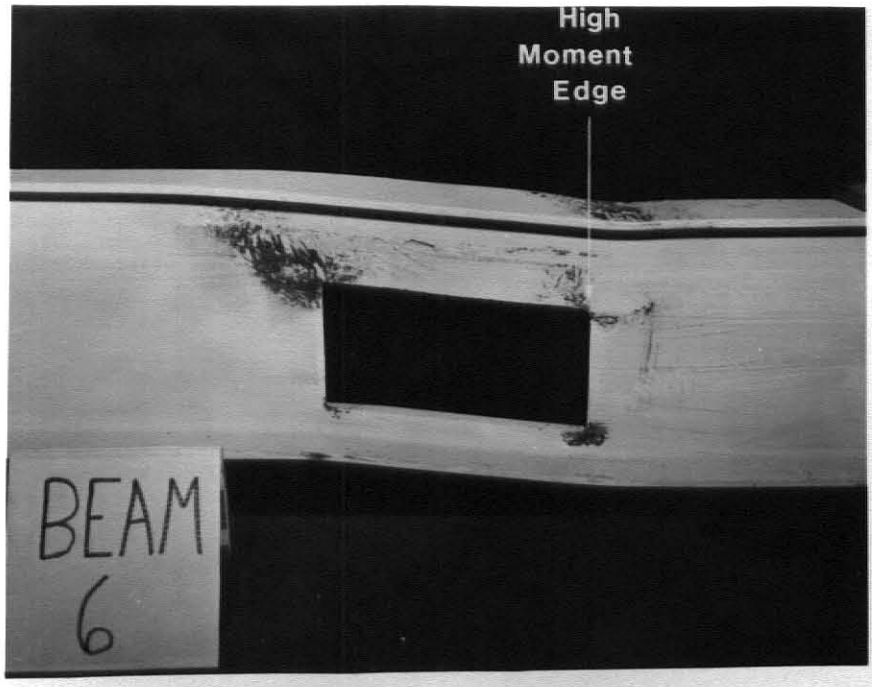


Figure 18a - Final Yield Pattern--Beam 6


Figure 18b - Web Buckle--Beam 6

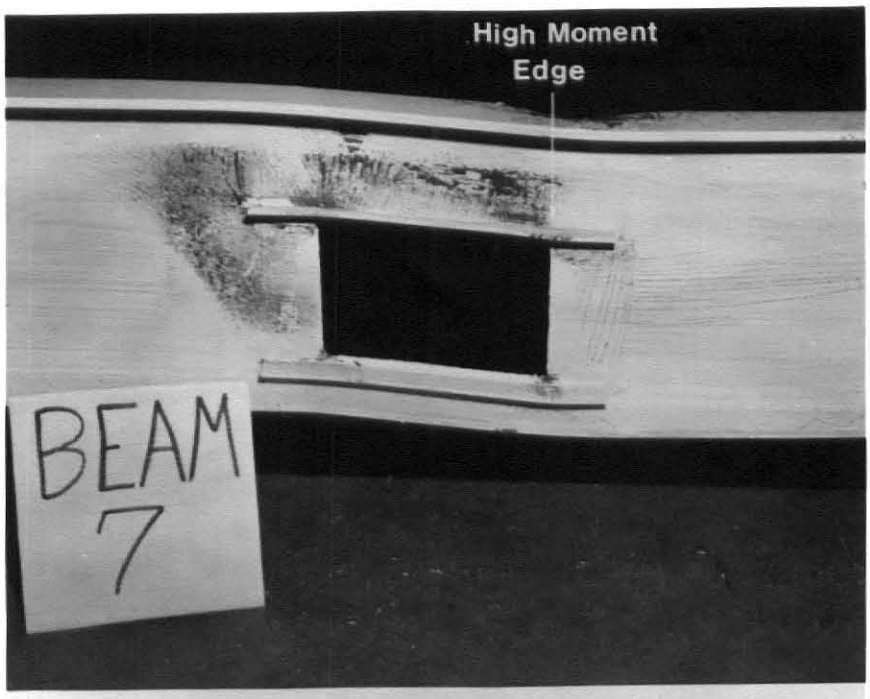


Figure 19a - Final Yield Pattern--Beam 7

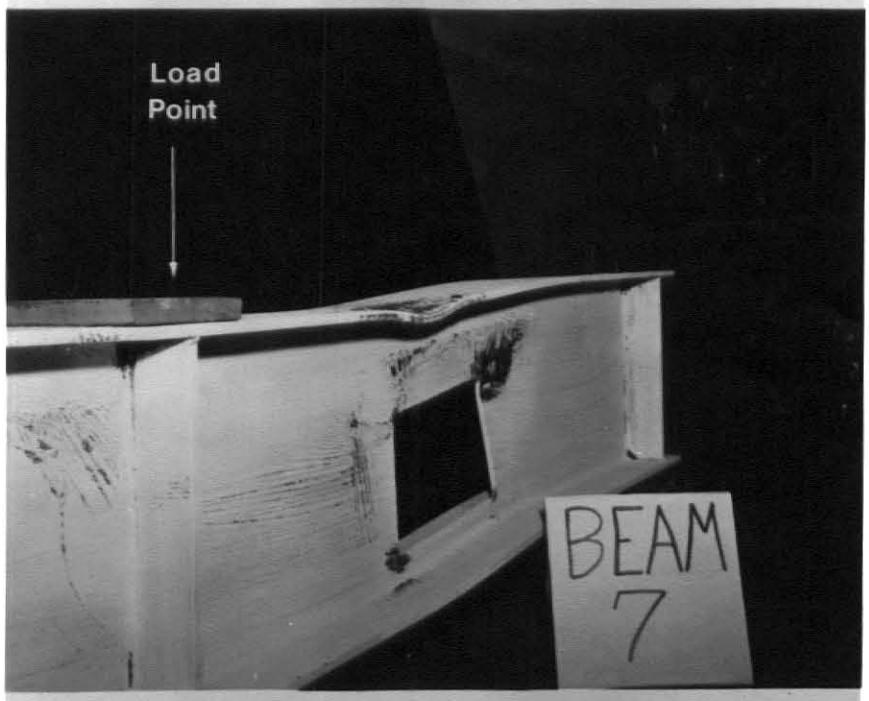


Figure 19b - Web Buckle--Beam 7

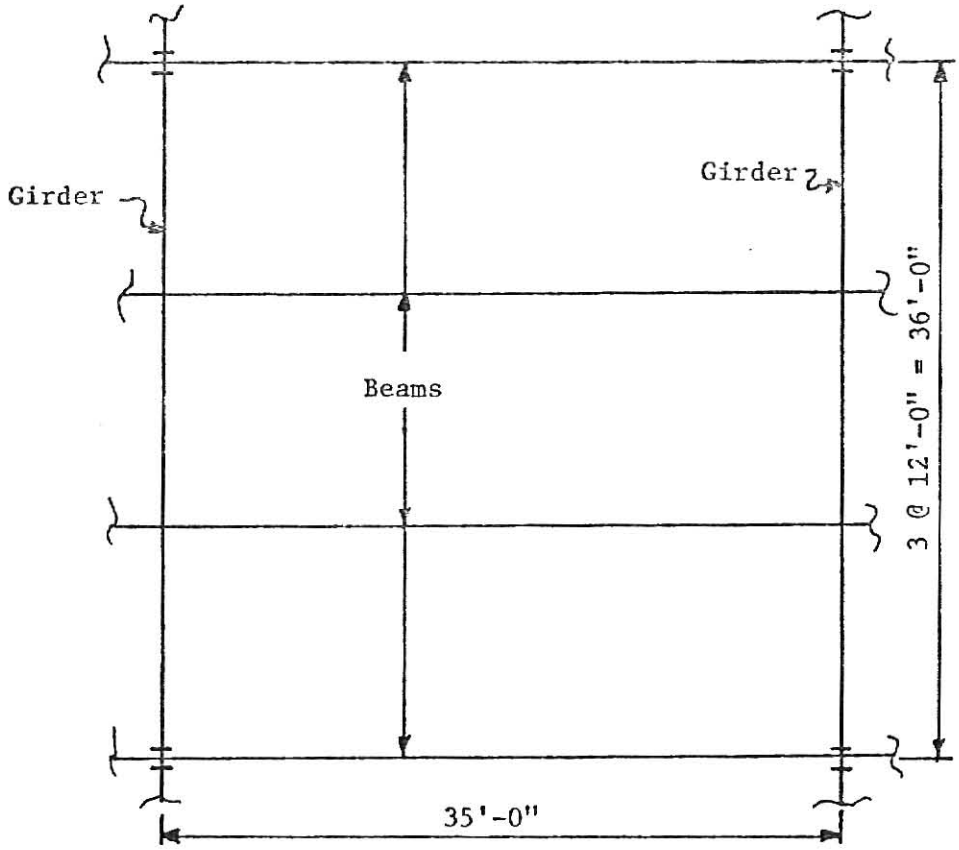


Figure 20 - Plan View of Floor System

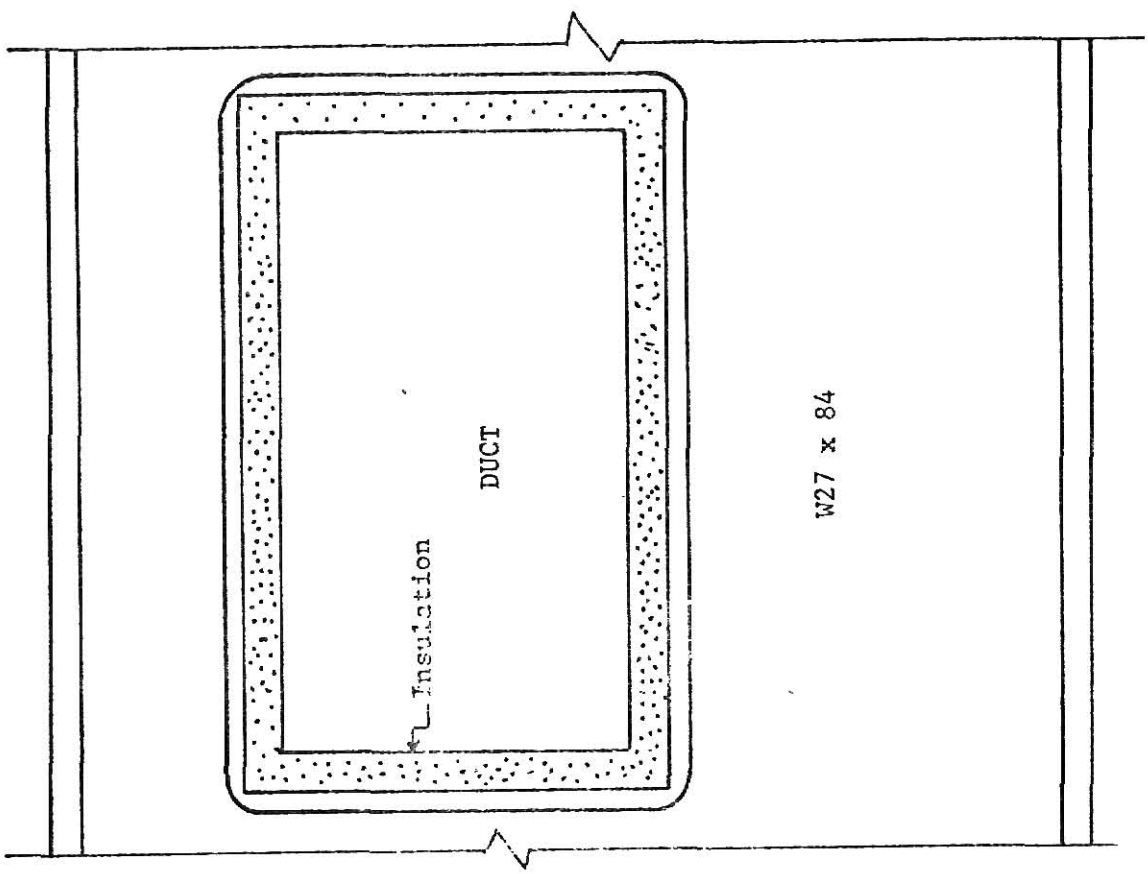


Figure 21b - Girder Elevation at Opening.

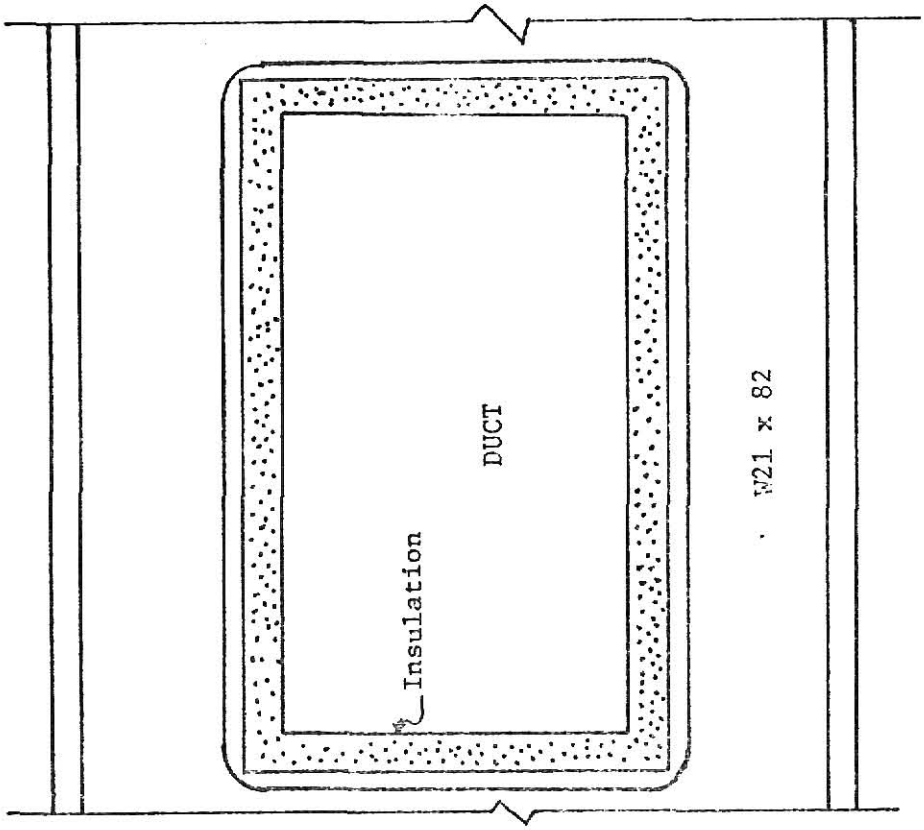


Figure 21a - Floor Beam Elevation at Opening.

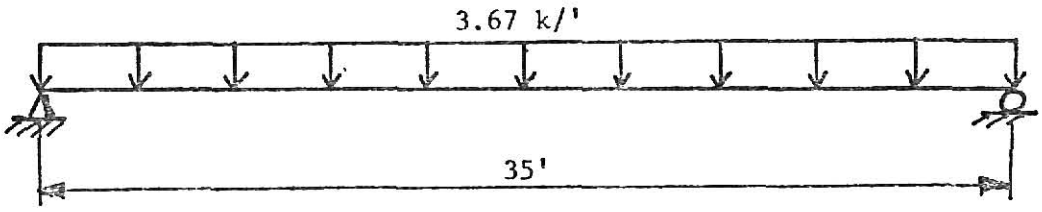


Figure 22a - Floor Beam Loading


Figure 22b - Floor Beam Shear Diagram

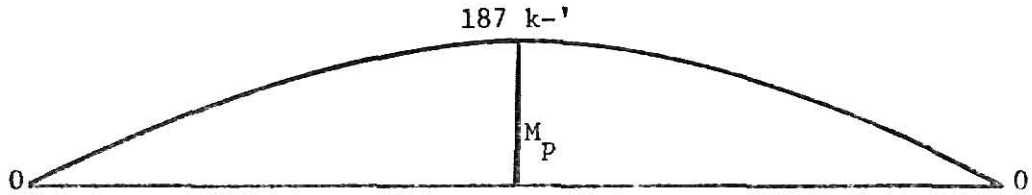


Figure 22c - Floor Beam Moment Diagram

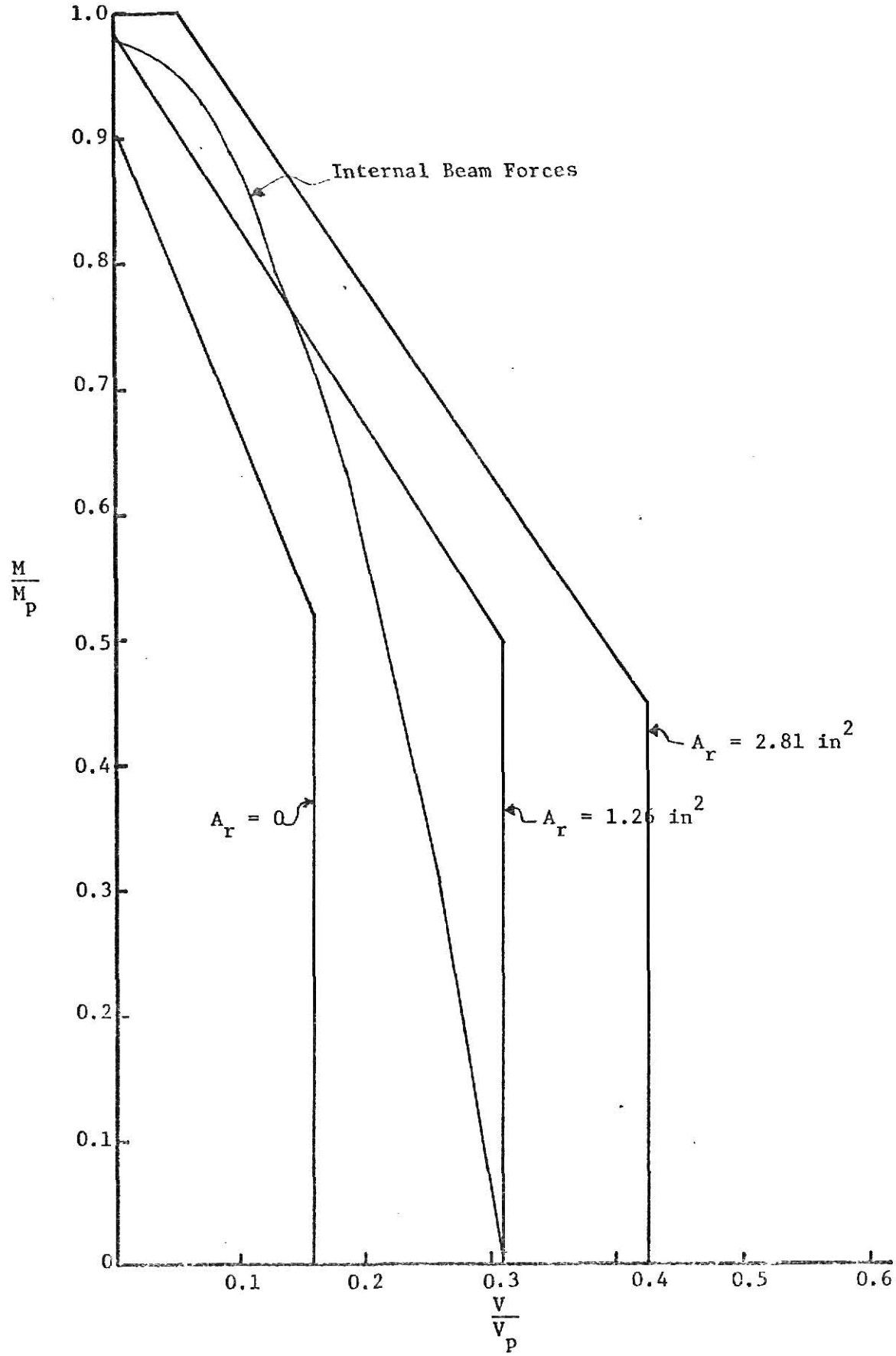


Figure 23 - Floor Beam Interaction Diagrams

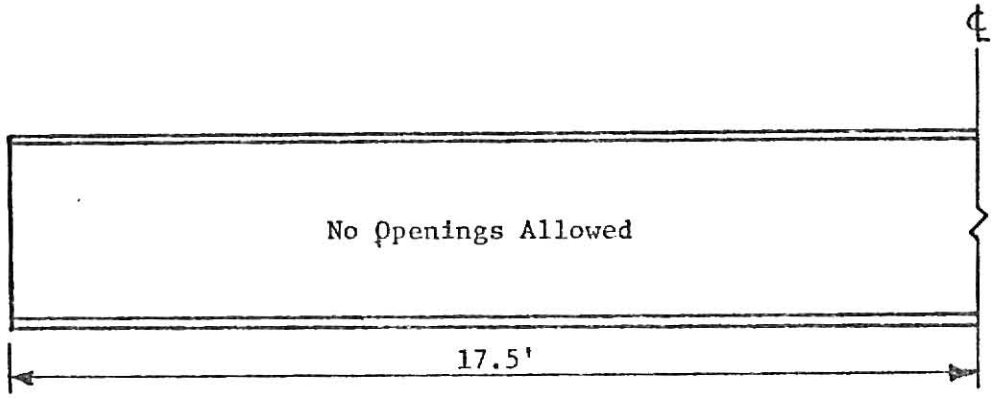


Figure 24a - Permissible Opening Locations for Floor Beams with $A_r = 0$

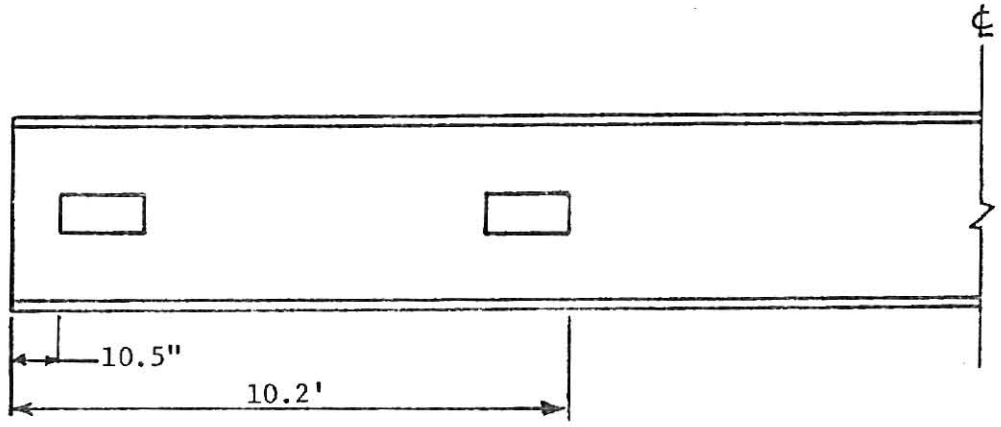


Figure 24b - Permissible Opening Locations for Floor Beams with $A_r = 1.26$ in$^2$

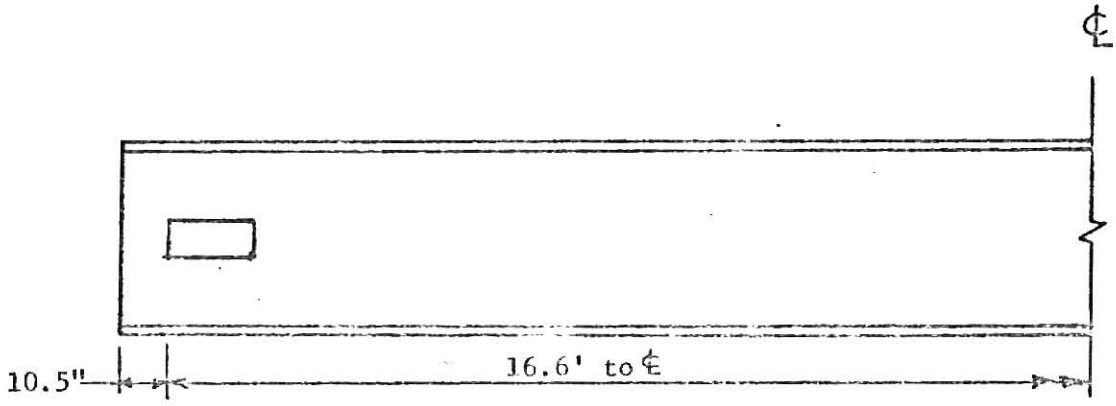


Figure 24c - Permissible Opening Locations for Floor Beams with $A_r = 2.81$ in$^2$

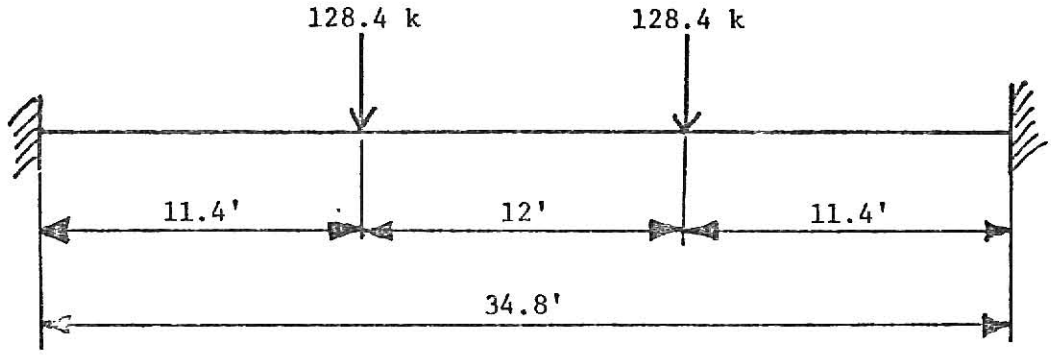


Figure 25a - Girder Loading

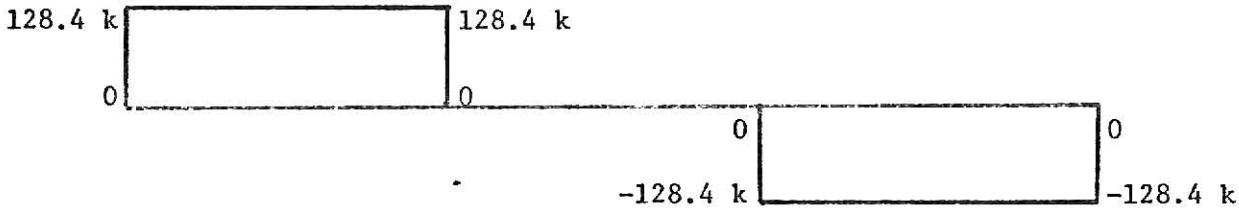


Figure 25b - Girder Shear Diagram

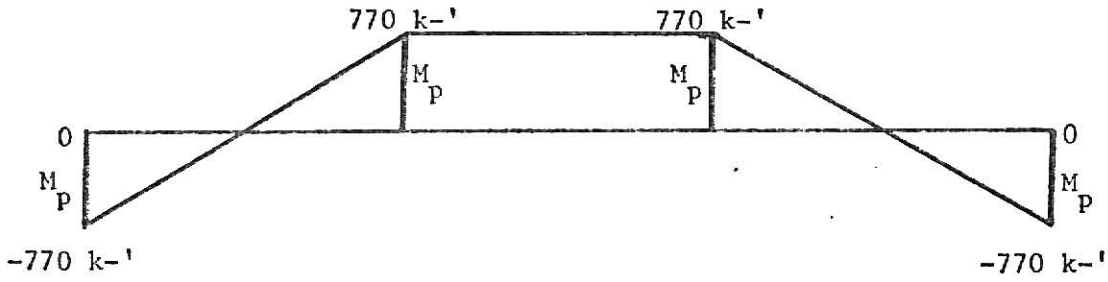


Figure 25c - Girder Moment Diagram

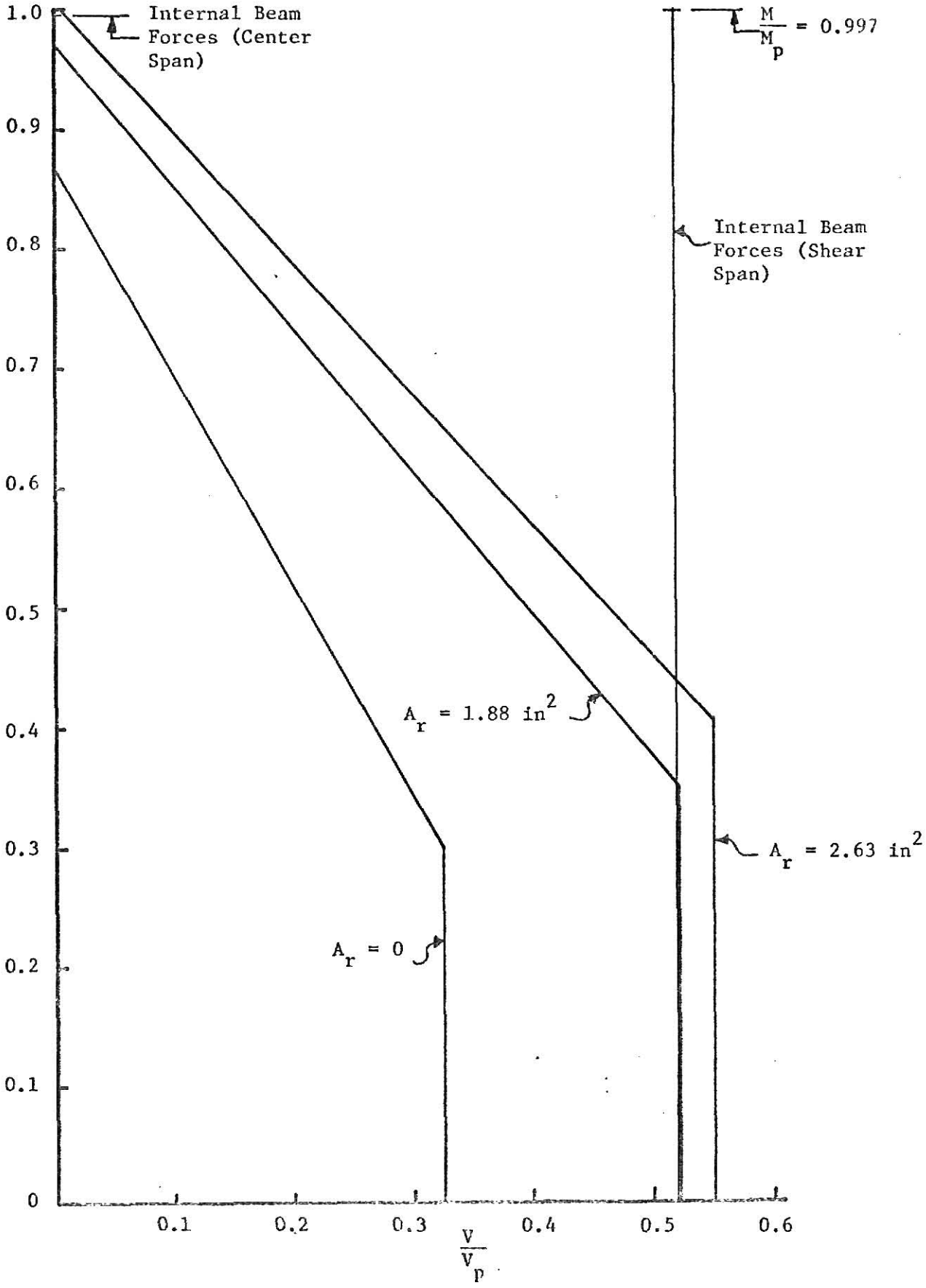


Figure 26 - Girder Interaction Diagrams

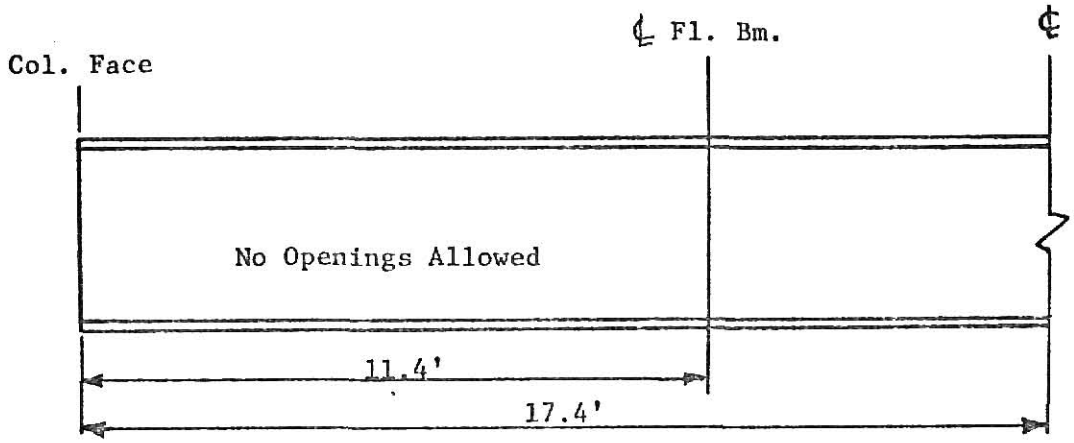


Figure 27a - Permissible Opening Locations for Girders with $A_r = 0$

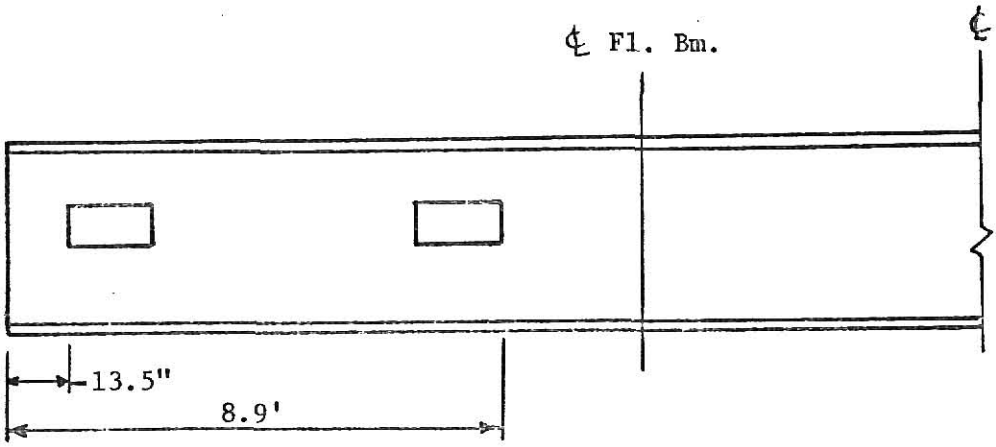


Figure 27b - Permissible Opening Locations for Girders with $A_r = 1.88$ in$^2$

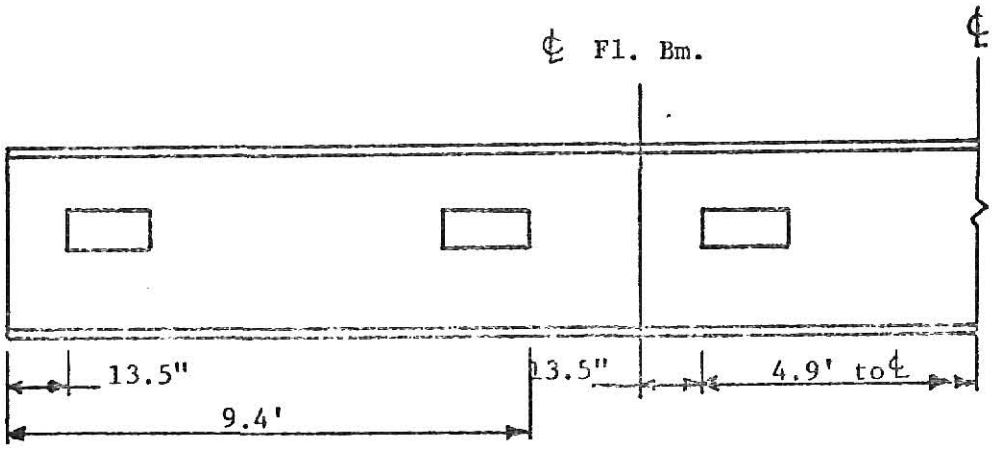


Figure 27c - Permissible Opening Locations for Girders with $A_r = 2.63$ in$^2$

# BEAMS WITH WEB OPENINGS: ULTIMATE LOAD TESTS AND DESIGN EXAMPLE

by

RICHARD LYNN KUSSMAN

B.S., Kansas State University, 1974

---

AN ABSTRACT OF A MASTER'S THESIS

submitted in partial fulfillment of the

requirements for the degree

MASTER OF SCIENCE

Department of Civil Engineering

KANSAS STATE UNIVERSITY
Manhattan, Kansas

1975

## ABSTRACT

In steel buildings it is sometimes necessary to position ducts for heating, ventilation, and air conditioning systems in the same space occupied by the steel beams and girders rather than below these members. For beams of varying depth it is more economical to use eccentric openings in some of the beams than to incorporate numerous vertical bends in the ducts.

Part I deals with ultimate load tests on five W-shape steel beams with eccentric web openings. The primary variables were the opening length, opening depth and reinforcement. The maximum loads sustained at failure and the failure modes are compared with theoretical values.

In Part II the use of previously developed design formulas for reinforced, eccentric web openings in steel beams is illustrated with a design example. The example deals with the design of part of a building floor system consisting of floor beams and girders with different depths.